Doctoral Dissertation

Development of self-reset image sensor with high signal-to-noise ratio for in-vivo imaging

生体イメージングに向けた高い信号対雑音比を有する自己リセットイメージセンサの開発

Thanet Pakpuwadon

September 2022

Nara Institute of Science and Technology

Division of Materials Science

Development of self-reset image sensor with high signal-to-noise ratio for in-vivo imaging

Thanet Pakpuwadon

Photonic Device Science Laboratory, Division of Materials Science

Nara Institute of Science and Technology

Supervisor

Professor Jun Ohta

Abstract

The nervous system regulates important bodily functions. It is crucial to comprehend its dynamics and functionality to prevent or treat brain-related diseases. Although numerous strategies for studying brain function have been developed, they remain poorly understood due to their complexity, and each method has limitations. Optical imaging is an essential technique for brain research. It allows the living brain to be closely observed. It has many functional interactions and changes to be investigated over many scales. A scanning microscope, such as confocal or two-photon microscopy, can image the exposed cortex at the cellular level. However, it is not suitable for a wide field of view. Besides that, fluorescence microscopy is a common method of studying the brain. These methods all face the same issue. The experimental setup with the microscope made it impossible to observe the animal while it was moving freely or exhibiting natural behavior due to the huge equipment setup. Several groups have created miniaturized devices to circumvent these constraints to solve such problems. These devices still utilize conventional microscope optics in combination. As a result, the necessary equipment, such as tethered and huge attached devices, occasionally obstruct the animal's natural behavior.

A complementary metal-oxide-semiconductor (CMOS)-based implantable optical imaging device is an alternative method for observing neural activity. At the same time, the subject is in motion and likely to perfectly solve the mentioned problems within the near future due to its powerful on-chip processing capabilities and cost advantage. Previously, our team has succeeded in developing ultra-small and lightweight implantable CMOS image sensors for contact imaging. Therefore, not only is it suitable for implantation, but it also has the potential to be an entirely wireless device in its compact size.

This time, we developed an image sensor to enhance intrinsic signal imaging. This method was chosen as an alternative way to study the mouse brain without having to take an extra step for genetic modification. Changes in signal intensity correlate with various brain states. Some crucial reactions in the mouse brain result in a minuscule signal change. Thus, a high-performance image sensor is required to detect those changes of approximately 0.1 percent. A signal-to-noise ratio (SNR) greater than 60 dB and high linearity are required to observe these small signals. Typically, the peak SNR of a typical active pixel sensor (APS) is 40–50 dB. It has a large number of image sensors designed for biological applications. Several image acquisitions approaches, including linear and logarithmic, well-capacity adjusting, dual or multiple sampling, multiple integration time, time-based, and self-reset procedures, have been introduced. However, the majority of the strategies have only enhanced DR performance. Due to the photodiode's limited well capacity, they haven't made much progress in increasing the peak SNR. Among the mentioned techniques, only the self-reset technique solves the well capacity limitation while also improving SNR.

In our previous research, Sasagawa *et al.* proposed using a self-resetting pixel to achieve a high effective SNR. With the improved version, Yamaguchi *et al.* obtained a high SNR of 64 dB, which can detect the hemodynamic signal from the mouse brain along with the stimulation. A Schmitt trigger inverter is used as a detecting circuit for pixel saturation in our proposed pixel. There are alternatives, such as a comparator based on a differential amplifier or an inverter chain, which suffer the cost of increased area consumption. The Schmitt trigger inverter has the advantage of only requiring a few transistors and less power consumption. Nonetheless, the experiment could be enhanced. If the device has a high enough effective SNR, it has a chance of receiving a higher-definition signal from the brain. We discovered that the active circuit connected to the V_{rst} has

insufficient stability and may result in a signal drop or a 3 dB increase in noise at the initial reset. Consequently, it has become a low offset for the SNR since then. This voltage drop must be minimized to increase the effective SNR.

This time, we present alternate methods for enhancing the self-resetting image sensor. One uses a modified photodiode structure to increase full-well capacity (FWC) to get an even better SNR. P-diff/N-well/P-sub was chosen as a photodiode because its physical structure has a greater thin layer area than that of a comparable-sized N-well/P-sub. This allows the pixel to manage more electrons per reset cycle. It minimizes self-resets and prevents the unstable phase. An alternative option is to use a MOS capacitor to increase a FWC and improve its linearity. In addition, a new relay board with improved performance was utilized. Additionally, we built image processing to minimize the system's artifacts.

Dedication

This thesis, as well as all the work that went into it, is dedicated to all the animals that have been and will be utilized in this research. The advancements I have made to the scientific method have been driven primarily by a concern for their well-being. May their sacrifice not be in vain, but rather lead to and contribute to greater good.

Pakpuwadon Thanet

Acknowledgments

This thesis is made possible by the generous support and assistance of numerous persons. I would want to convey my sincere appreciation to everyone for their active guidance, cooperation, and support. Without the following individuals, this thesis would not be feasible.

I would like to thank Professor Jun Ohta for providing me with the opportunity and continuing support to pursue a doctorate at Nara Institute of Science and Technology. Because of his intellectual abilities, he is one of the reasons I chose to pursue a master's degree and doctorate at NAIST. Without question, I have never once regretted making this choice. Not only does he provide me with academic help, but he also supports me in other areas and consistently gives me excellent life counsel.

I would also like to thank Associated Professor Kiyotaka Sasagawa for his advice, encouragement, and vast expertise. He consistently supports my work. Working with such a highly skilled professional researcher is an absolute pleasure. I could not have envisioned a finer adviser than him.

In addition, I would like to express my deepest gratitude to the members of my thesis committee, Professor Masakazu Nakamura and Professor Takayuki Yanagida. I owe them an enormous debt of gratitude for the invaluable insight and advice they have provided me with regard to my work over the past three years.

I also would like to thank Professors Takashi Tokuda (Currently a professor at Tokyo Institute of Technology), Toshihiko Noda (Currently an associate professor at Toyohashi University of Technology), Hiroyuki Tashiro, Makito Haruta, and Hironari Takehara for their insightful comments and discussions. I would also want to thank the members of the Photonic

Device Science Laboratory for their gracious hospitality and unwavering support. I am especially grateful to know Mrs. Ryoko Fukuzawa and Dr. Yasumi Ohta, our laboratory's secretary and post-doctoral fellow, respectively. They support, love, and care for me as if I were a member of their family.

To YOU and anyone who landed their eyes on this paragraph, either by accident or on purpose, this is the most lively part of this document. It is not connected to the paragraph before or even after. If you are seeking something within this part of the thesis, it is just here for you. With a kind of fear, I decided to stop my time here just to prepare and learn to move on. Spend it for several years. It's just to realize things that you may have figured out 10 years ago. The passage of time had equipped me with the necessary things to go on. Finally, I considered it worthwhile. Leave me a question for the rest of the time and hints to challenge myself to prove that within remains. My heartfelt thanks go to you for always being supportive and kind. Out of the names had mentioned before, a lot of people have come and gone. Ones have just come to pass, and some have bonded. Thank you for the 'personal family', sure that family, and the ones following, Kulachatr, Wuttinan, Thanaree, Krittaphorn, Champ, Ton, May, Pai, and Ben, as an emotional support and sense of security. Leave it here, my acquired wisdom. "Nothing is worth your physical or mental health." Just throw it away because I want you to be the happiest person on the planet. Leave it here, another promise that this time would never be the same. "It's on me, everything will be fine."

Lastly, but most importantly, I would want to convey my deepest thanks to my family for their love, support, and encouragement during my years of study and the process of conducting research and producing this thesis. My parents are the primary force that keeps me going and from quitting. This accomplishment would not have been achievable without their help.

Disclaimers

All animal handling procedures and experimentation were approved and under control by the Nara Institute of Science and Technology (NAIST) Animal Committees and were performed in accordance with the institutional guidelines of the animal facilities of NAIST.

Contents

List of Figures

Chapter 1 Introduction

1.1 Research background

The brain is among the most intricate organs. Almost all the creatures use their brains for memory, learning, and emotional expression. It controls nearly all bodily functions. These brain functions have been realized by a neural network of more than 100 billion nerve cells communicating via trillions of synapses. But how does it work? What if we can fully comprehend it? We discovered that understanding brain function could help in treating neurodegenerative diseases. Long-term, a deeper understanding of brain circuits is likely to yield new treatments for debilitating brain diseases. Consequently, there is a great need for brain imaging technologies to examine animals and their natural behavior.

The measurement of brain neuron activity in freely moving mice is expected to be a significant step forward in revealing brain functions. Implantable devices for electrical or optical measurements allow for monitoring neuronal activity in the awake brains of mice and rats. Optical neural recording techniques have been promising tools in recent years. The optical approach has various advantages over standard electrophysiology, including the absence of electrical noise and the simultaneous imaging of a wide region, number of neurons, or selective recording from genetically targeted neurons. The optical neural recording technology includes both intrinsic and extrinsic optical recordings. Intrinsic neural recording methods use small changes in optical properties of brains to emphasize the dynamic reaction, such as blood flow and oxygenation, cellular volume change, or refractive index change, without external indicators [1].

To understand how the brain processing in mammals, animals must be able to interact with their environment in entirely natural behavior. Therefore, there is a high demand for implantable

devices to observe the mouse brain in an awake condition. Some groups have developed new devices to observe the correlation between brain functions and behavior. **Figure 1** shows head-fixed imaging and a compact head-mounted device developed for calcium imaging in moving mice [2], [3]. Most of them are based on a miniaturized microscope system with an image sensor that is commercially available or employing an optical fiber in combination with the microscope [2]–[6].

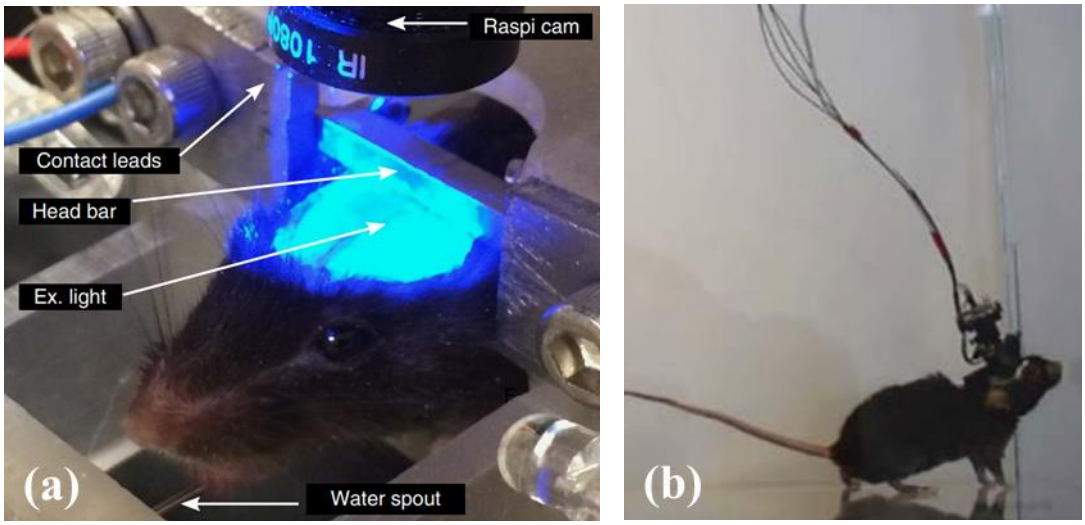

Figure 1 (a) shows a head-fixed mouse for performing brain imaging. (b) shows a head-mounted imaging device for freely moving mouse [2]**.**

1.2 Problem statement

Even though various devices have been developed to handle these experiments, most of the devices still require large and heavy equipment in combination or in the form of tethered devices. The awake mouse can sometimes be learned, but only in the head fix condition due to the required equipment. The wiring of the tethered device also hinders the entirely natural behavior of the mouse in the situation. Therefore, the best solution is to apply completely wireless devices, whose weight, size, and high accuracy or high signal-to-noise ratio (SNR) must be

considered. However, before realizing such a novel device, the imaging module, as the most important part of the device, still needs more development.

1.3 Research purpose

This thesis proposed the latest version of the self-reset image sensor with an extremely high SNR to become the intrinsic signal imaging device. The SNR is reached at over 70 dB, which is higher than the 60 dB required to perform intrinsic signal imaging [7]. I also demonstrated an *in-vivo* imaging device implementing this self-reset image sensor for blood flow imaging. The new smart buffer board to work with the image sensor and the latest developed image processing techniques are also used in this research for the first time.

To gain an even higher effective SNR, I utilize self-resetting techniques along with enlarging the full-well capacity (FWC) of the image sensor pixel. This time, I introduce two methods for enlarging the FWC. One is using the modified photodiode structure to increase the capacity of the photodiode itself. The P-diff/N-well/P-sub structure was chosen as it gives higher FWC than the N-well/P-sub structure, which is usually used. Another method is for the FWC to be enlarged by introducing a MOS capacitor in the pixel. Both strategies yield different outcomes, which will be discussed throughout the thesis.

These prototypes in this study are significant steps toward the ideal device for *in-vivo* imaging in freely moving animals. Because of its design, which is tailored to a specific application, this image sensor has not only a sufficiently high SNR but also a small size and light weight. The architecture inside was designed to optimize power consumption, which is closely related to the heat in the system that must be concerned with the implantable device. Thus, it potentially is implemented in the imaging module of the ideal wireless imaging device within the near future.

1.4 Thesis overview

In this section, a brief overview of the thesis was provided. This thesis has five chapters, which are shortly explained below.

Chapter 1: Introduction

This chapter serves as a synopsis of the thesis. A brief history of the research theme and how it came to be demanded of this special CMOS image sensor is clarified. The current problems and limitations of brain imaging are then discussed. Then, the goal of this study is to solve the problems that have been identified.

Chapter 2: Brain imaging overview and Self-reset image sensor

A literature review is given about the devices that have been implemented and a brief history of this research theme. This chapter discusses a few techniques commonly utilized in brain imaging and the demand for innovative imaging devices that can break through barriers. We also introduce the idea of a self-reset image sensor here in this chapter as it is used for the other applications and leads to the concept of our techniques. There is a history of our self-resetting CMOS image sensors. This chapter talks about the past improvements and limitations of the self-reset image sensor. It also talks about the in-vivo experiment that used the self-reset image sensor to successfully image the brain.

Chapter 3: Self-resetting image sensor utilizing the modified structure photodiode method and MOS capacitor method

The most recent version of the self-resetting image sensors would be present. Both utilizing the modified structure photodiode method and the MOS capacitor method will be discussed in this

chapter, including the new relay board and evaluation. The state-of-the-art benefits of this advancement are discussed. Finally, linearity and FWC are defined.

Chapter 4: In-vivo imaging and Image processing

After the evaluation is complete, the self-reset image sensor is assembled into the in-vivo imaging device and demonstrated in the experiment that is performed with the anesthetized and head-fixed mouse for the blood flow imaging. The apparatus used in the experiment are discussed. The necessary image processing that this image sensor requires is revealed in this chapter. The final image is displayed and leads to the discussion.

Chapter 5: Conclusion, and Future of this work

The final chapter of this thesis summarizes all the research results and concludes the outcomes of the thesis. Following that, potential avenues for future research are discussed.

Chapter 2 Brain imaging overview and Self-reset image sensor

2.1 Optical imaging of the brain and observation of neural activities

Mammalian brains use sequences of action potentials in a huge population of neurons to process complex information such as sensations, movements, and difficult cognitive activities. Brains use neural networks made up of over ten billion neurons to process such complex signals at the same time. Individual neurons are known to have hundreds or thousands of synaptic connections with other neurons. Therefore, the functions of individual neurons or connections are challenging to investigate because of these intricate connections [1].

This chapter briefly reviews the representative optical techniques for in-vivo neural signal imaging in brain research. We first present the current methods for detecting extrinsic neural signals using calcium indicators and the latter method that applies intrinsic signal imaging, which comes from the change of the natural optical properties of the hemodynamics. These are for being a background for our device properties and pointing out that the compact high performance imaging device is needed. After that, we introduce the concept of the self-resetting image sensor through the existing research.

2.1.1 Extrinsic optical signal imaging using calcium indicator

Using activity-dependent fluorescent proteins, such as calcium indicators and voltage-sensitive dyes, has become popular in recent years [8]. It's primarily because of the development and improvement of the optical detecting device that turns physiological signals into changes in fluorescence and the development of a suitable device for detecting fluorescence. Combined with

genetic modification approaches, these extrinsic optical signals are becoming a powerful tool for studying neural signaling in cultured neurons, brain slices, or even living animals [9]. Consequently, the recording of somatic calcium signals is frequently used to monitor neuronal action potentials. Since during the resting state, the intracellular calcium concentration in most neurons is maintained at less than 100 nM, whereas it increases 10 to 100 times during the formation of action potentials [10]. Thus, monitoring these changes can emphasize the correlation between dynamic brain activity and specific stimulation.

To monitor the calcium signal based on brain activity, several devices and approaches were developed for this application. As mentioned, it is necessary to observe the brain while it is in natural behavior. Therefore, various head-mounted devices have been developed [2], [5], [11], [12] and also a lot of techniques using optical fiber [13].

2.1.2 Intrinsic signal optical imaging

Intrinsic optical signal imaging is a technique for measuring physiological changes associated with neuronal activity without an additional procedure for labeling. This is because intrinsic signal imaging is derived from the changes in the optical properties of neural tissues. Small alterations detect the intrinsic signal imaging in reflected light in the blood flow, the oxygenation of hemoglobin, the cellular volume, and the membrane potential from physiological changes in the brain. Therefore, Intrinsic optical signal imaging measurement mainly indicates cerebral blood volume (CBV) [14], [15].

It was also combined with other methods like flavoprotein autofluorescence imaging (FAI) to calibrate the result that it was mixed with the hemodynamic signals [16]. Numerous biological and medical research have utilized green fluorescence imaging (e.g., GCaMP calcium indicator

and also flavoprotein autofluorescence imaging, FAI) to better understand the mechanisms of brain activity during resting and stimulation states [17], [18]. During functional brain imaging, hemoglobin in cerebral blood flow (CBF) also absorbs green fluorescence. Thus, the CBF response could significantly impact the green fluorescence signals derived from the activation of neuronal during the study.

In order to eliminate the effects of light absorption on the signal during brain activity, a study has devised a correction technique for green fluorescence imaging. The compensating method's fundamental principle is that CBF affects the light absorption rate. To get rid of this fluctuated the CBF. Intrinsic signal imaging could be applied and detect the quantity of the absorption quantity that was affected by the CBF. Consequently, if they simultaneously measure FAI and intrinsic signal imaging in an animal's brain, the effects of CBF's light absorption on FAI signals can be compensated by parallel intrinsic signal imaging. The diagram in **Figure 2** shows how the study work to compensate for FAI with intrinsic signal imaging. In conclusion, they effectively demonstrated accurate estimation of brain function independent of hemodynamics, indicating that this method can be used to estimate brain function in animal models of stroke and dementia. To perform this parallel imaging, they use the scheme of the head-fixed experiment as shown in **Figure 3**.

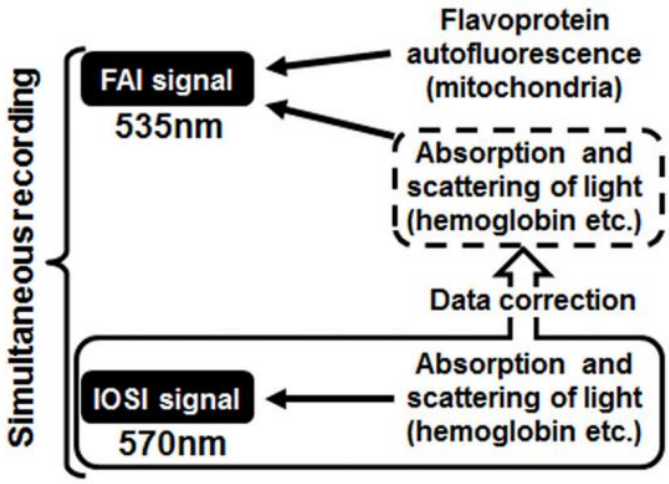

Figure 2 A schematic diagram of the correction method. The absorption and scattering effects of cerebral blood flow contained in the flavoprotein autofluorescence imaging (FAI) signal were removed [16]**.**

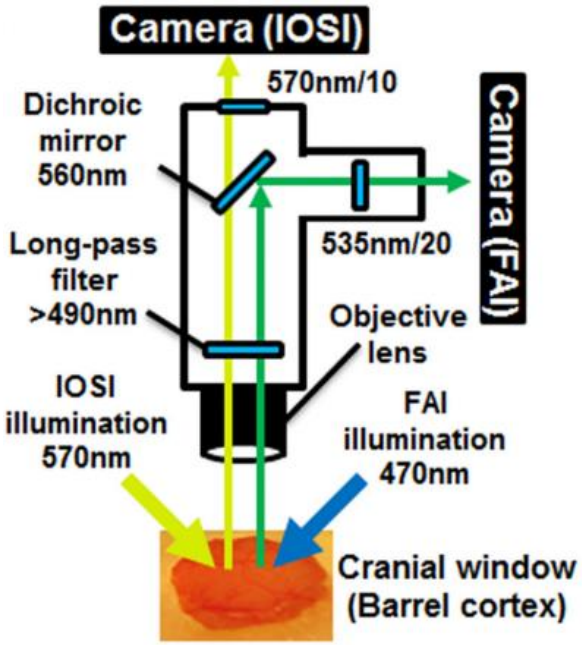

Figure 3 shows Diagram of the experimental apparatus used for simultaneous flavoprotein autofluorescence imaging (FAI) in parallel with intrinsic optical signal imaging (IOSI). This process also relies on additional preparation cranial window to expose cortical [16]**.**

The result is that the FAI measurement was frustrated and pulled down by the CBF. Thus, it could be compensated by deducting the consequence of the intrinsic signal imaging, which detected mainly the CBF. The imaging result is shown in **Figure 4**.

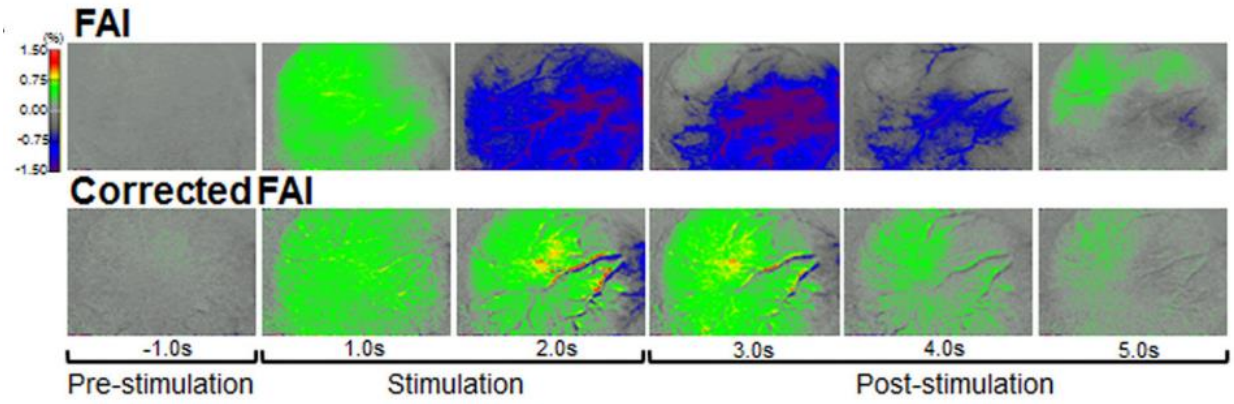

Figure 4 shows the result of the parallel imaging [16]**.**

From **Figure 4**, an uncorrected FAI shows the percent change of the signal that the CBF pulls down. After the compensation, it shows that the correct value from the FAI measurement has a lot lower peak than the uncorrected FAI.

2.2 Optical Imaging Devices for in-vivo observation

2.2.1 Calcium imaging using a head-mounted device

Calcium-imaging techniques also use the mountable device, making it possible to observe the target neurosignal in a moving mouse. The head-mounted module is portable and can be carried by an adult mouse, which allows the mouse under study to move freely in an arena. Rely on the commercial imaging module, and the following is one of the most recently head-mounted devices designed for calcium indicator imaging technique. The device breakdown, appearance, and head-mounted setup are shown in **Figure 5** [2].

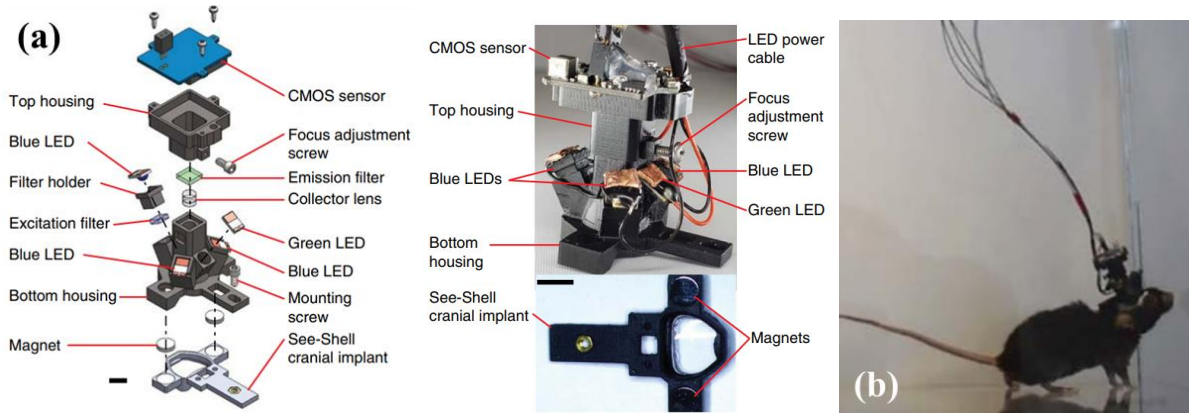

Figure 5 (a) One of the most recent head-mounted devices, which also relies on miniscope, the well-known commercial imaging module. (b) An imaging of a mouse wearing the head-mounted device and engaging in natural behavior [2]**.**

Figure 6 shows another example of the miniaturized microscope being a head-mounted device [11] These devices still mainly rely on the scheme of a miniaturized microscope, which mainly uses the commercial imaging module as an imaging part. This device is designed for volumetric calcium imaging.

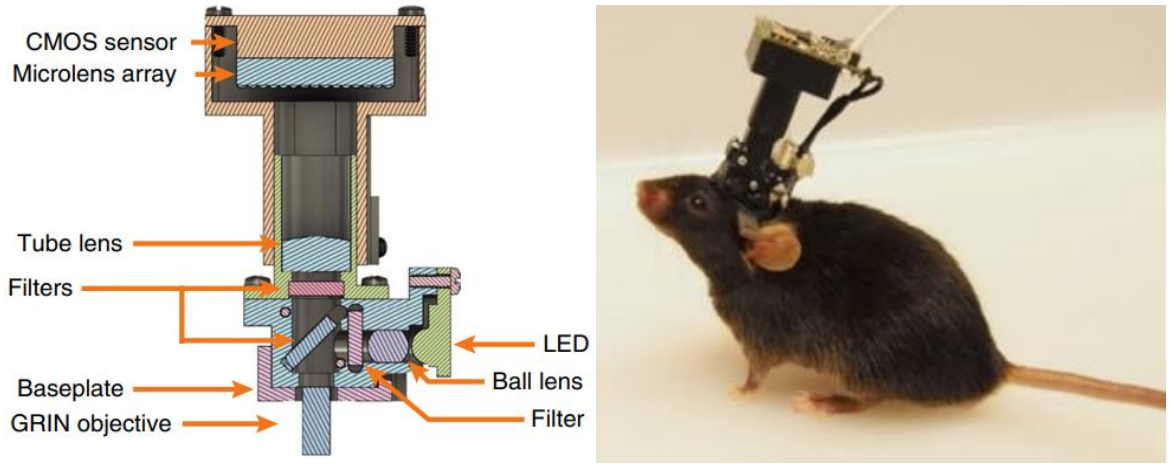

Figure 6 (Left) shows the diagram of the calcium imaging device, which is capable of volumetric imaging. The device is a combination of head-mounted miniscope technology and light field microscopy. (Right) an adult mouse with the head-mounted device attached [5]**.**

As shown in **Figure 5** and **Figure 6**, the design of the device is bulky. It occasionally obstructs the mouse behavior in some postures or activities, including noise or error in the data due to the device design and its unstable setup. This bulky system is a penalty from housing design to handle the optic system. Since the imaging module still needs a lens in combination.

2.2.2 Contact imaging with implantable CMOS image sensor

To comprehend normal brain activities during animal behavior, such as motion and sensing, a technology for optical imaging of the brain under conditions of free movement is crucial. The majority of brain imaging investigations employ anesthetized laboratory animals. This brain imaging equipment is too large for experimental animals such as rats. According to reports, the neuronal activity of the brain differs between non-anesthetized and anesthetized states. Therefore, to understand the biological neural activity corresponding to animal behavior, we need an imaging technique of the brain functions under freely moving conditions.

This is where contact imaging takes place. These imaging techniques could be implemented without concern for the optical system. Thus, its imaging part is a very compact device and is suitable for in-vivo imaging in behavioral experiments. In our group, we can design an implantable CMOS image sensor for contact imaging in freely moving conditions[19]–[23]. **Figure 7** depicts a contact imaging image sensor developed by our group. The input and output signals of the sensor were transmitted to a control board through a relay board using four wires. As shown in **Figure 7**, our image sensor typically requires at least 4 pads for the clock, VDD, ground, and output. Basically, for controlling the image scanning and the data output from the imaging [24]–[26]. This image sensor was based on a 0.35-μm CMOS standard process. The miniaturized imaging device implementing this image sensor chip is described in **Figure 8** and **Figure 9**. The specification of the chip is shown in Table I.

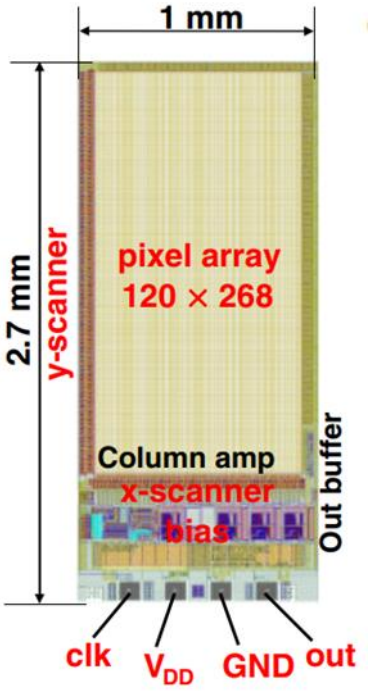

Figure 7 Layout of an image sensor to be mounted on contact imaging module [24]**.**

Table I Specification of the 4 pads image sensor developed by our group

Technology	0.35-μm 2-poly 4-metal standard CMOS process
Operating voltage (V)	3.3
Chip size (μm^2)	1048 × 2700
Pixel array size (μm^2)	900 × 1920
Pixel type	3-transistor active pixel sensor
Photodiode	N-well/P-sub
Pixel size (μm^2)	7.5 × 7.5
Fill factor (%)	44

The operational amplifier and digital buffer on the relay board were utilized to regenerate the attenuated signals. As the sensor output is an analog signal, the control board was equipped with an analog-to-digital converter for transferring the signals to a personal computer (PC) for control and measurement. The sensor's analog output signals were transformed into 14-bit digital information. Using a custom PC application, the signals were acquired and analyzed. In the contact imaging procedure, the surface of the imaging device would be contacted by the brain surface directly. Figure 8(a) represents the graphic of in-vivo imaging device employing this image sensor, which attached to the polyimide cable (Taiyo Industrial). This design separates the imaging portion of the device from the controlling portion or relay board, making imaging configuration easier. Figure 8(b) shows a diagram of the imaging setup. The image sensor is attached to the brain surface directly and illuminated by built-in LEDs.

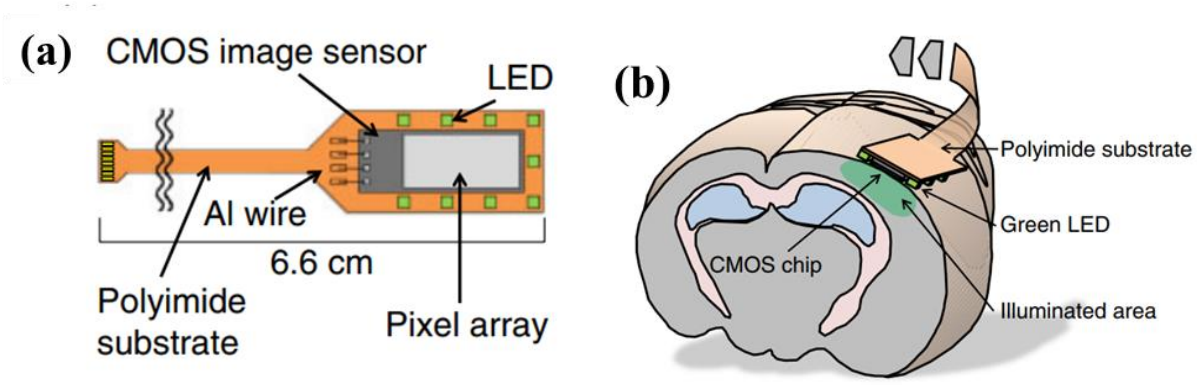

Figure 8 shows a diagram of an imaging device using this image sensor, which is surrounded by 9 LEDs for the illumination. (a) An overview of the device imaging part. (b) Graphic shows implementing of this image sensor with built-in illumination [24]**.**

The lateral imaging part in **Figure 9(a)** shows the real iamging decive. It connected to the controller board. This stretched imaging part not only reduces the invasiveness of the implantation site but also less restricts the movement of the animals. Moreover, it will make it easier to implement in multiple device imaging experiments. **Figure 9(b)** depicts the imaging part attached to the brain surface with the LED turned on for self-illumination.

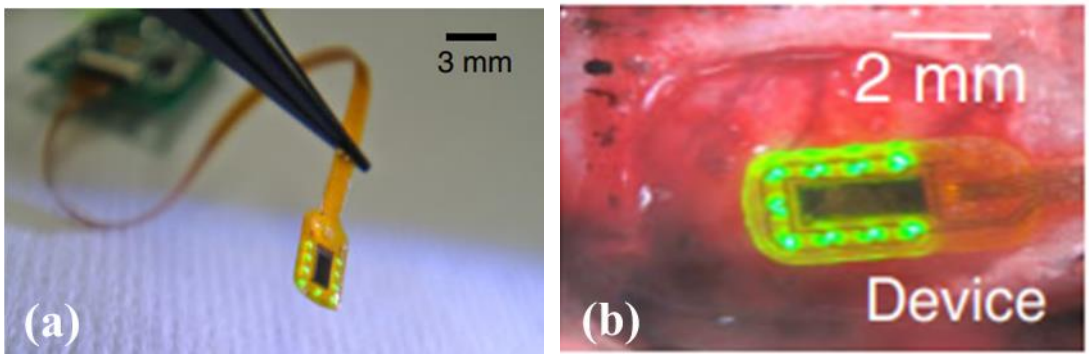

Figure 9 (a) The appearance of the in-vivo imaging device, including its controlling part, which is connected to the PC. (b) The imaging device contact directly to the brain surface [24]**.**

The imaging process is simplified because only the imaging part is involved. A view of the surface of the brain through a microscope is shown in **Figure 10**. The area marked in **Figure 10** contains the imaging location that comes from this sensor. The image obtained from the device while still inside the living organism is displayed here. In this example, the rat must be anesthetized, and its head must still be fixed to the stereotaxic equipment. The target area's skull and dura were removed. Removal of the dura allowed for precise observation of the vessels on the surface of the brain.

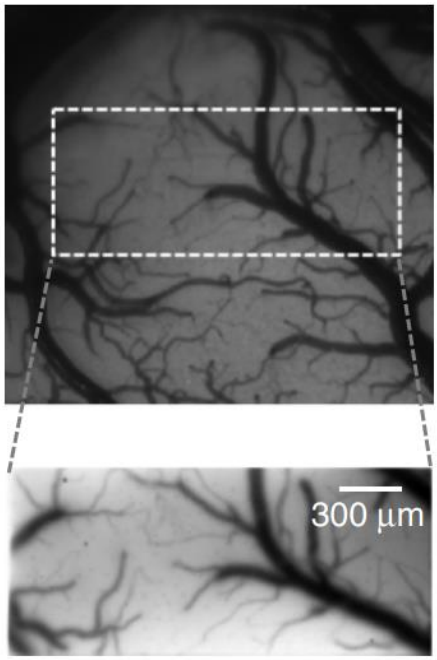

Figure 10 Image of the brain surface taken by the microscope shows the target area for contact imaging and image captured by the imaging device was show [24]**.**

2.3 High SNR image sensors

At a particular input level, the SNR is the ratio between the signal and the noise. The SNR is represented by the equation below.

$$SNR = 20\log\left(\frac{Signal}{noise}\right)\ [dB]$$

Therefore, to increase the peak SNR, the noise source must be inspected in order to provide overcoming strategies. As theoretically suggested in **Figure 11**, a virtual image sensor was used to simulate noise in the CMOS image sensor, consisting of photo-conversion characteristics, photon shot noise, and read noise (noise floor) as a function of incident photons.

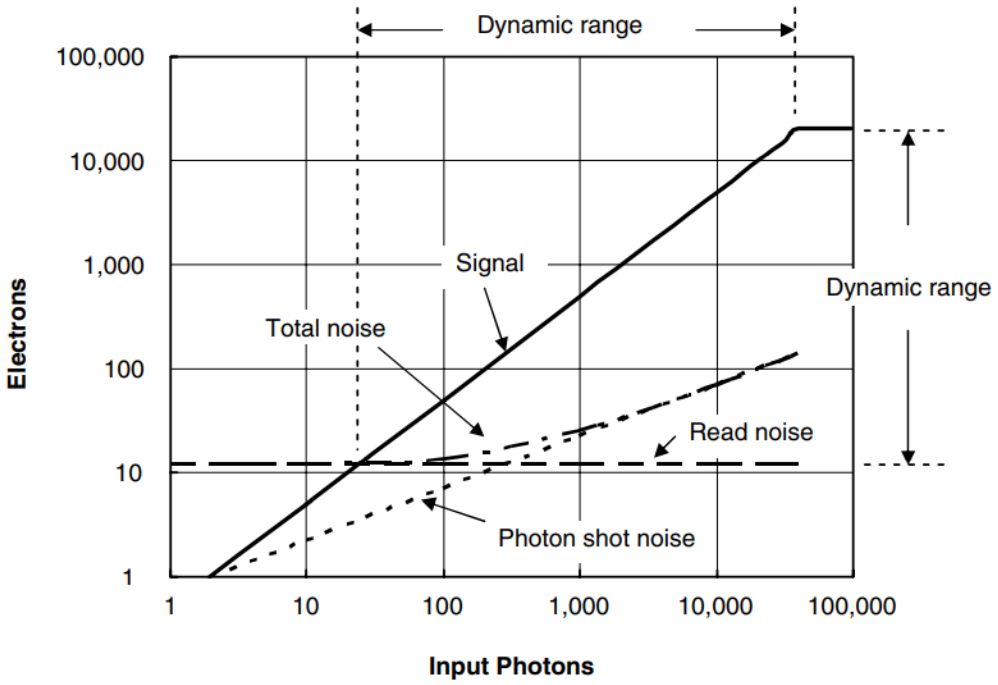

Figure 11 Photon shot noise and read noise as a function of incident photon [27]**.**

When photons strike the detector, they generate free electrons, and the movement of these electrons generates a measurable electric current or photo current. Shot noise in the current measurement results from the unpredictable character of these free electrons. The number of electrons generated will fluctuate at random in every given time interval. According to the Poisson statistics for uncorrelated random discrete events, the standard deviation of the average number of electrons generated randomly in a given time interval, n, is equal to the square root of *n*. Hence, the photon shot noise can be calculated by the equation.

$$\sigma_{Shot\ Noise} \simeq \sqrt{n}$$

The photon shot noise increases with the light intensity and is only dominant when it is higher than the read noise. Thus, it caused the limitation in the high light intensity region, as shown in **Figure 12**.

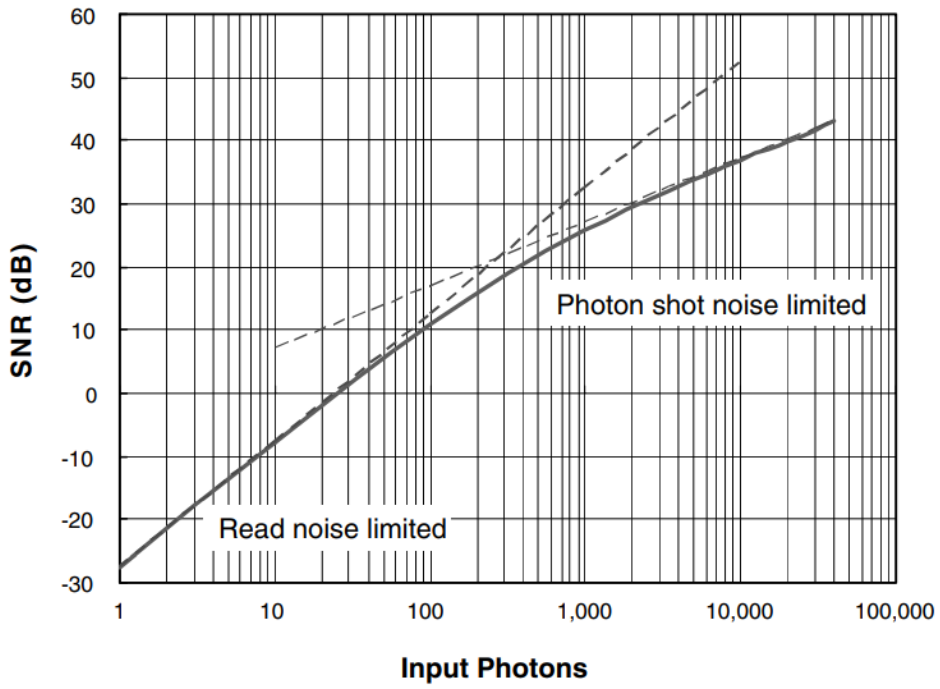

Figure 12 SNR as a function of incident photons of the typical image sensor [27]**.**

Due to the photon shot noise limit, the typical or conventional image sensor has a peak SNR of approximately 50 dB because of the size of its FWC [27]. This FWC is the maximum amount of charge that can accumulate on the photodiode's capacitance. When this photodiode capacitance is full of the charges produced by photons, it is saturated and unable to measure any additional light signals.

2.4 High FWC image sensors

FWC is the parameter that limits the peak SNR in the typical pixel. Various strategies were developed to enlarge the FWC. In terms of pixels with high full-well capacitance, there were pixels with high FWC designed to realize a high dynamic range to handle such a specific function. The existing high FWC pixel will be present in this section.

Due to the fact that some imaging techniques, such as full-field optical coherence tomography (OCT), require a very high SNR and sufficient high resolution, an image sensor with an unusually high FWC was manufactured for this use [28]. This image sensor uses pixels that were designed for high FWC, which can handle $2Me^-$ with a 12 μm pixel pitch. It was interesting since the FWC was enlarged by implementing a MOS capacitor. The pixel schematic is shown in **Figure 13**. A parallel MOS capacitor is added to the photodiode to achieve the required FWC. The image sensor was fabricated by 0.18 μm CMOS image sensor process. The application of this image sensor is so close to the concept of the self-resetting pixel since it aims to be used in a high SNR region where photon shot noise is the dominant noise. The low SNR response region of the OCT image sensor will typically be clipped.

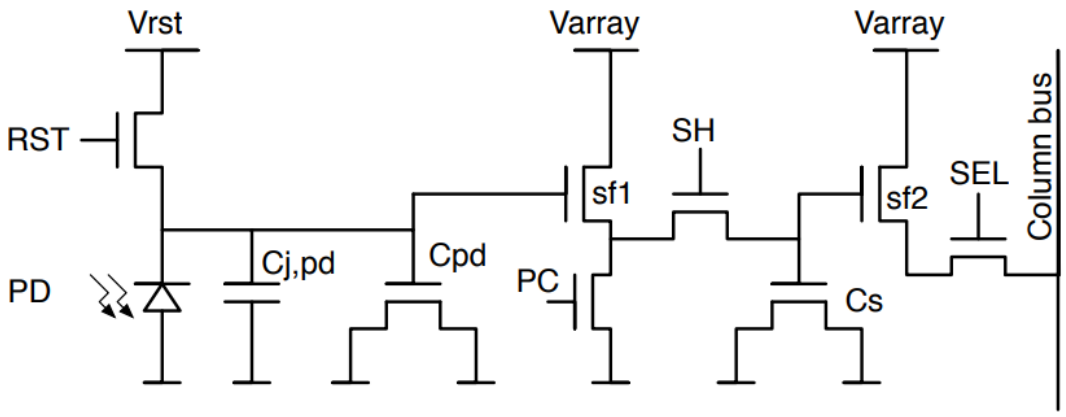

Figure 13 Pixel of the global shutter image sensor with 2Me⁻ FWC [28]**.**

Though the CMOS image sensor process was used, a regular n-well/p-sub structure can be used as a photodiode. Because the benefits of lower dark current and lower read noise offered by pinned photodiodes are not essential for the OCT application and it is hard to achieve in the available pixel pitch. The fill factor is 25% even the fine process was used due to the penalty of introducing the MOS capacitance. The final image acquired from this high FWC pixel was shown in **Figure 14**.

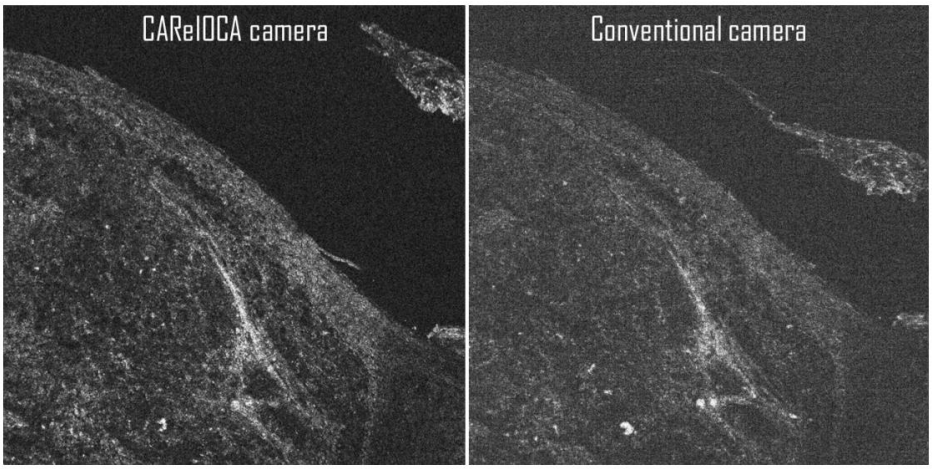

Figure 14 OCT image obtained using image sensor using high FWC of 2 Me⁻ (left) and a typical image sensor with a 90 Ke⁻ FWC (right) (LL Tech) [28].

Another interesting technique was reported. It is the image sensor designed for achieving extremely high DNR using a novel design called lateral overflow integration capacitor (LOFIC) [29], [30]. This image sensor was also designed using the 0.18 m CMOS image sensor process. This technique introduces the additional capacitors and is called an overflow capacitor, which is connected in parallel with the floating diffusion (FD). **Figure 15** illustrates the pixel schematic. To achieve such a high DNR, the overflow capacitor was controlled by a switch so that the flooded electrons from the FD could be stored in this additional capacitor. The pixel layout is shown in **Figure 16**. The pixel size is 16×16 μm^2.

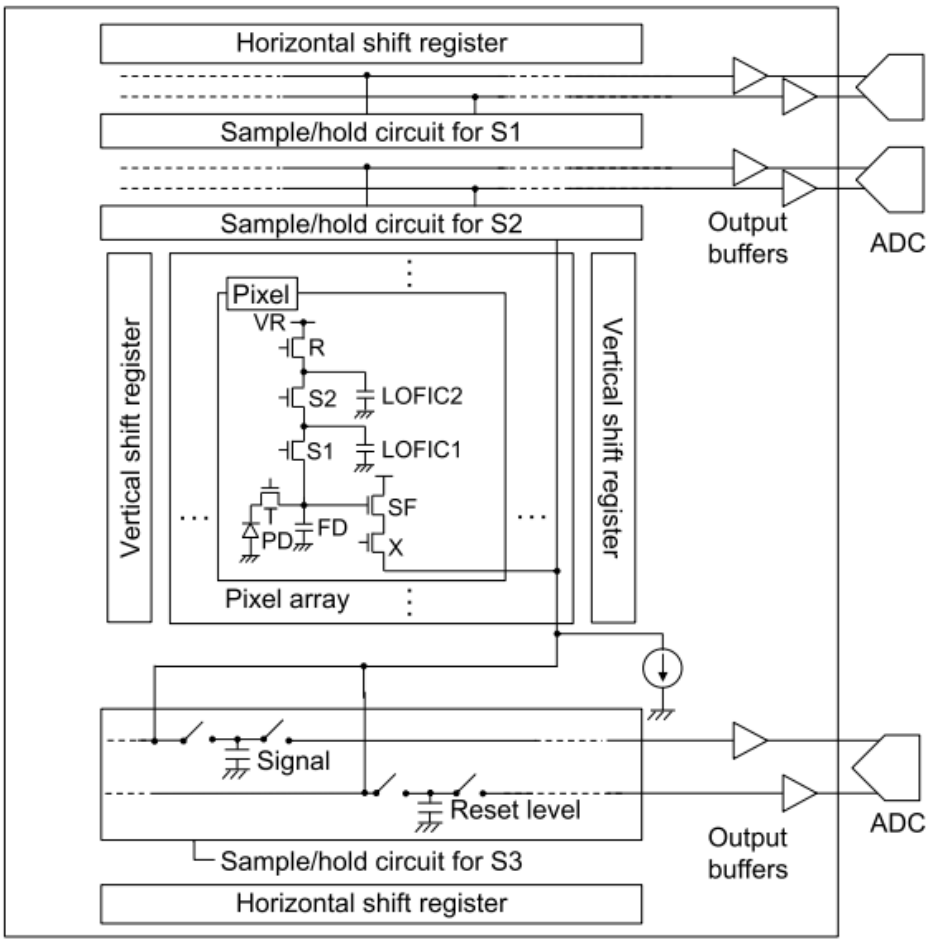

Figure 15 The block diagram of the image sensor with two-stage LOFIC [30].

From **Figure 15**, the overflow capacitors are shown as LOFIC1 and LOFIC2 in the pixel schematic. As shown in figure 16, the fill factor is 52.8% fabricated by the fine process. The 30% of the pixel was occupied by the overflow capacitor as LOFIC1 and LOFIC 2.

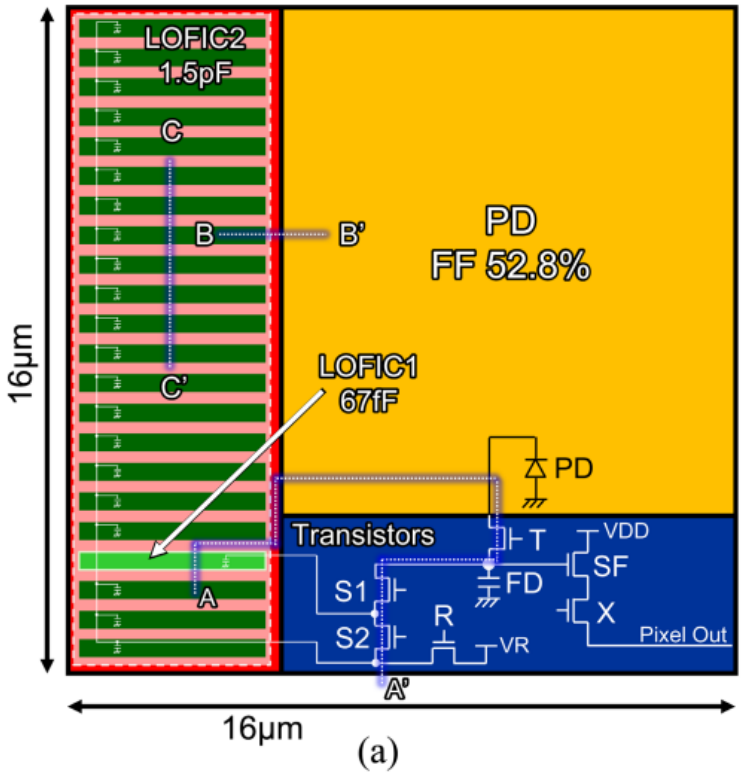

Figure 16 Layout of the pixel with LOFIC shows that it occupies 30% of the pixel area[30].

Figure 17 shows the measured SNR characteristics of the image sensor with two-stage LOFIC. A maximum SNR of 70 dB was achieved at high DNR by switching to the LOFIC2 stage.

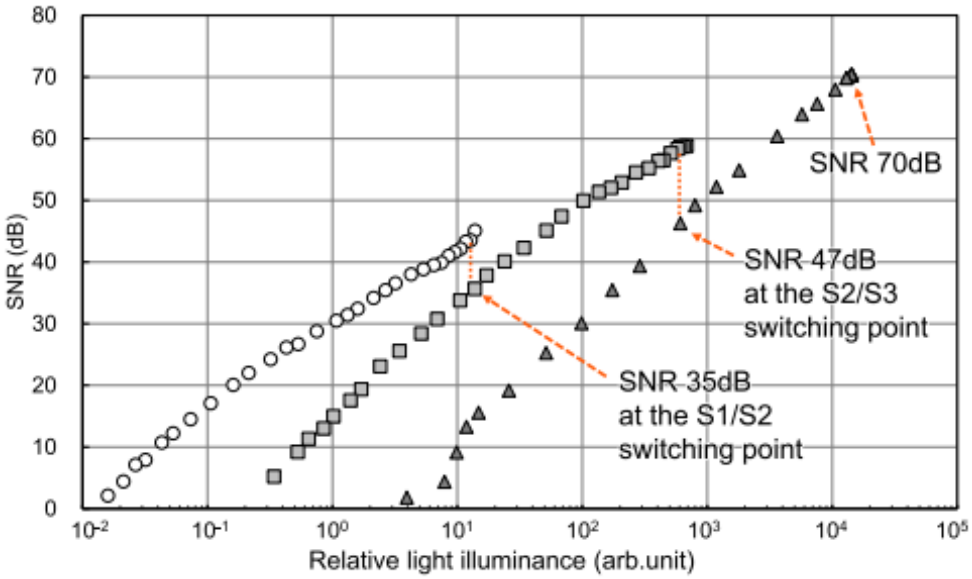

Figure 17 SNR characteristic of the LOFIC image sensor. The discontinue plot is due to the state switching [30].

2.5 The existing self-reset image sensors

The advantage of the CMOS image sensors is the ability to implement signal processing circuitry within the pixel. Self-resetting pixels can avoid pixel saturation and effectively increase the FWC. In such cases, pixel saturation is quite a challenging issue in CMOS image sensors. The pixel saturation also causes a limit in dynamic range (DR), the ratio between the largest and smallest photocurrent that a certain quantity can be measured. This photocurrent is the charge generated by absorbing photons. The amount of charge is handled by the pixel's FWC. There are many research efforts to increase the DR of CMOS image sensors. Various image-acquiring strategies were introduced, including logarithmic [31], multiple integration time [32], dual or multi-sampling [33], time-based [34], and self-reset techniques [35]–[40]. Among these techniques, the self-reset technique was particularly outstanding. This technique works by overcoming the limitations of the FWC. Thus, it can achieve improvement in both DR and SNR. Therefore, it may be advantageous for in-vivo imaging functions that demand a high SNR and DR.

The existing image sensor with a self-resetting function from the other groups would be displayed to familiarize with the pixel design and overview of the image sensor. The existing self-reset image sensor was designed for various functions. The following is counted as a digital pixel sensor (DPS) based on a pulse width modulation scheme (PWM) [35]. This design aims for a wide operating range with low power consumption. The schematic and layout of this self-resetting pixel are shown in **Figure 18**.

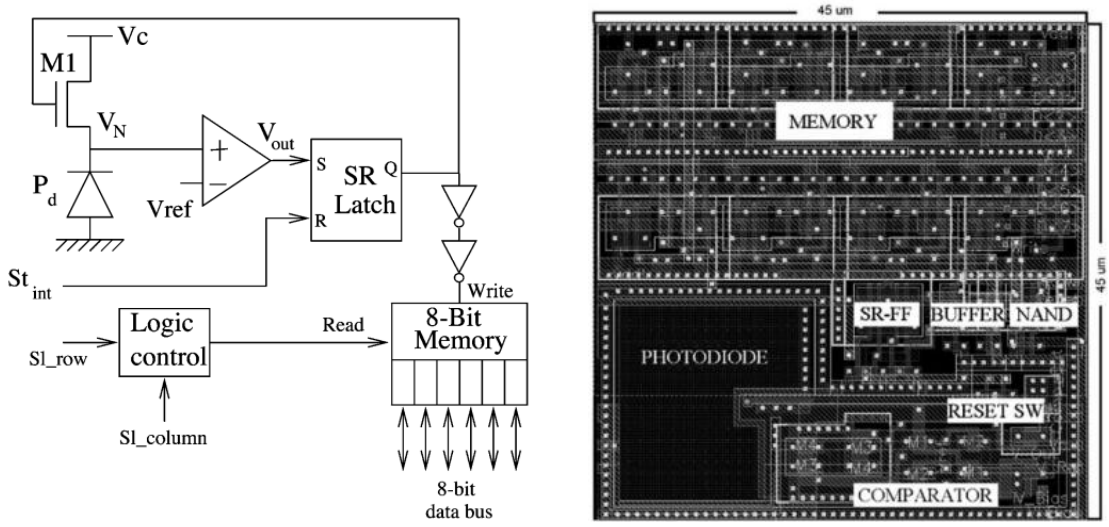

Figure 18 (a) The digital pixel block diagram. (b) The pixel layout with totally 45×45 μm² [41]**.**

With PWM, it seems the pixel has a built-in ADC on the pixel. Using a Gray counter, the photocurrent signal is encoded as a pulse-width signal and converted to an 8-bit digital code. Then it was stored in on-pixel storage. The DR of the pixel can be adjusted via modulating the counter circuit. This pixel has a wide and adjustable DR. However, the design takes a penalty from including the digital circuit into the pixel. The chip is fabricated by the 0.35-μm CMOS standard process. The fill factor is 12%, and the pixel size is 45×45 μm². The comparator and digital latch control its signal level for triggering the self-reset function.

The next CMOS image sensor implementing the self-reset technique increased DR and peak SNR performance [36]. Utilizing 0.18 μm CMOS process, the pixel fill factor is 50%. The pixel layout is shown in **Figure 19**.

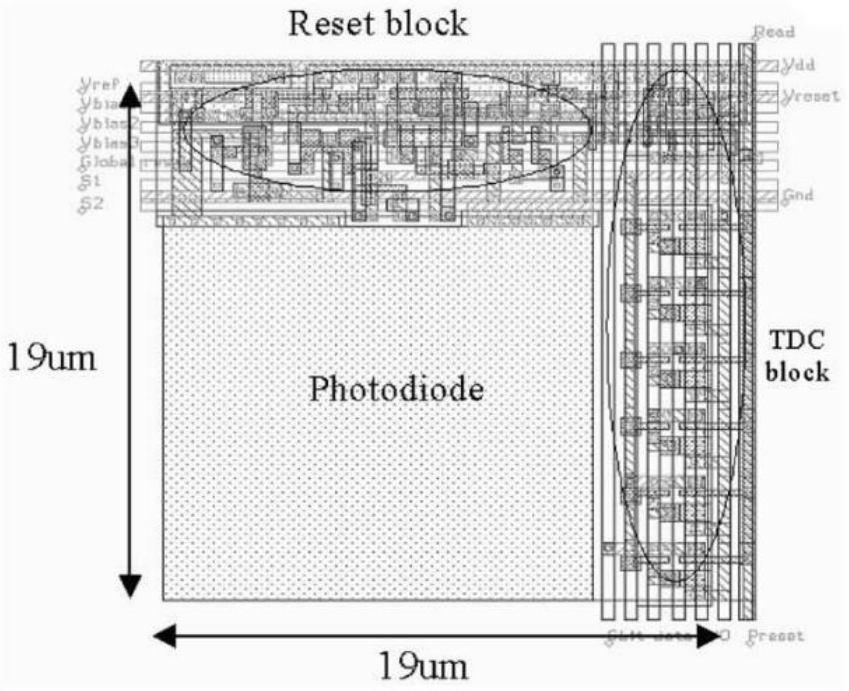

Figure 19 The layout of the self-reset pixel fabricated by 0.18 μm CMOS process [40]**.**

This pixel consists of a photodiode, a reset block, and a time-to-digital converter (TDC) block. Focusing on the reset block, it has a comparator, a bistable half-latch, and a regenerative switch to restart the integration. A schematic of the reset block in combination with TDC is shown in **Figure 20**. In this case, the resetting numbers are required for acquiring the image. Thus, the reset counting circuit is included. The most important aspect of this design over the others is the SNR performance improvement since the other methods have limited SNR performance due to the limited FWC of a photodetector.

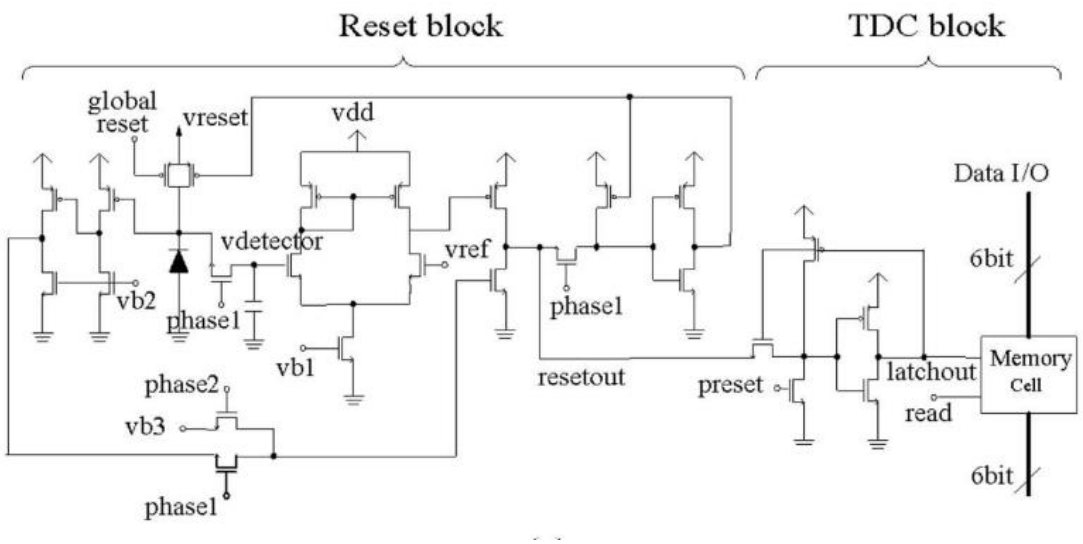

Figure 20 Schematic of the Reset block and the TDC block. This circuit features built-in counting the number of resets and analogue-to-digital conversion (ADC) [40]**.**

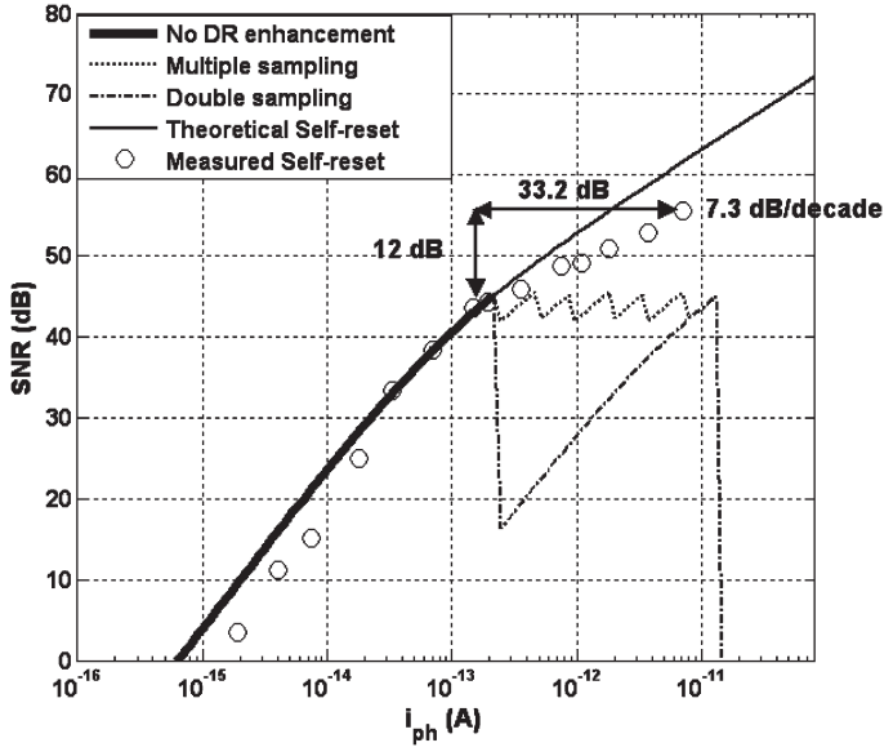

Figure 21 shows SNR performance compared with the other approaches [40]**.**

By the methods, this pixel has quite a large FWC. Thus, noises along the light intensity could be analyzed. According to the result in **Figure 21**. The readout noise and reset noise seem to be dominant over the shot noise in the low light intensity conditions. The difference from the theoretical trends is slightly overestimated from the pixel's readout noise. At high light intensity conditions, Photon shot noise becomes the main noise source, and the peak SNR trend is getting close to the theoretical curve. The SNR keeps increasing proportionally to the photocurrent and the high light intensity without saturation. However, it was found that the peak SNR occasionally drops due to the self-reset noise accumulation, which includes the self-reset time delay and also the crosstalk from the switching and comparator.

2.6 Self-reset image sensors for in-vivo imaging

In the previous research, we propose a complementary-metal-oxide-semiconductor (CMOS) image sensor with a self-resetting system with a high SNR to detect a small intrinsic signal such as a hemodynamic reaction or neural activities in the mouse brain. However, one strategy to improve the performance of this image sensor is to increase its FWC. In this study, the two most recent generations of advancements will be examined. Using a modified photodiode structure is one technique, while the most recent generation employs MOS capacitors. In conjunction with the image sensor, a buffer board is required. Thus, the most recent PCB board is displayed. Before going through the latest achievement, background and brief history of the self-reset image sensor are provided. Finally, we will describe the differences between our design and the self-reset image sensor developed by the other group.

Previously, we proposed and demonstrated an implantable CMOS image sensor with self-resetting pixels [42]–[46]. The self-resetting function is implemented using a four-transistor

Schmitt trigger inverter. The pixel has no counter for the number of self-resets because the application does not require a radiometric (linear) response. The pixel is fabricated using the 0.35-μm 2-poly 4-metal standard CMOS technology, which results in a pixel size of 15 μm × 15 μm and a fill factor of 31%. The effective peak SNR is more than 60 dB. This is quite enough for intrinsic signal detection arising from hemodynamic responses in a living mouse brain. The target area of the proposed self-reset CMOS image sensor performance is shown in **Figure 22**.

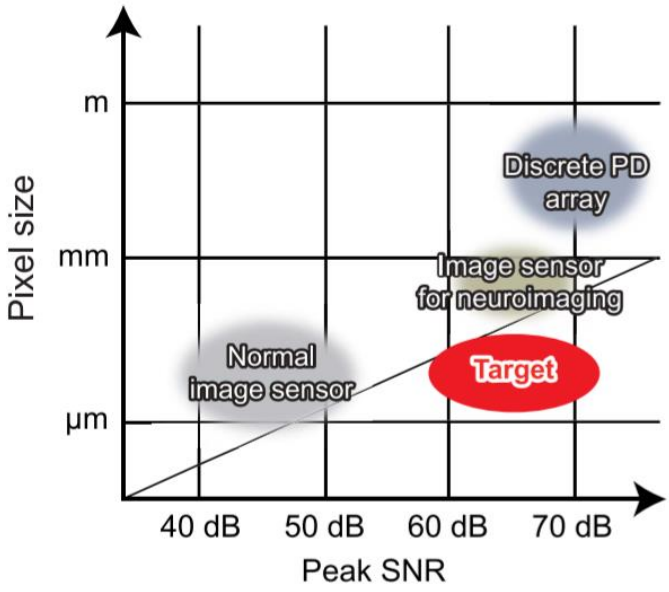

Figure 22 Target area of the self-reset CMOS image sensor compared to the other image sensor [42]**.**

An implantable imaging device was fabricated to detect local conversion between oxyhemoglobin (HbO) and deoxyhemoglobin (HbR) in brain tissues. An imaging experiment of hemodynamic responses in the cortical sensory area accompanied by forelimb stimulation of a living mouse was demonstrated. The implantable imaging device for intrinsic signal detection is expected to be a powerful tool to measure b rain activities in living animals used in behavioral analysis.

We employ a Schmitt trigger inverter as a self-reset level sensing circuit. There are other alternatives, including a comparator based on a differential amplifier and an inverter chain. A benefit of the Schmitt trigger inverter is its small number of transistors. It allowed allocating more pixel space to the other component. **Figure 23(a)** shows a Schmitt trigger inverter circuit we used. As a simple comparator, this group of circuits will detect when the voltage of a photodiode (PD) falls below a threshold.

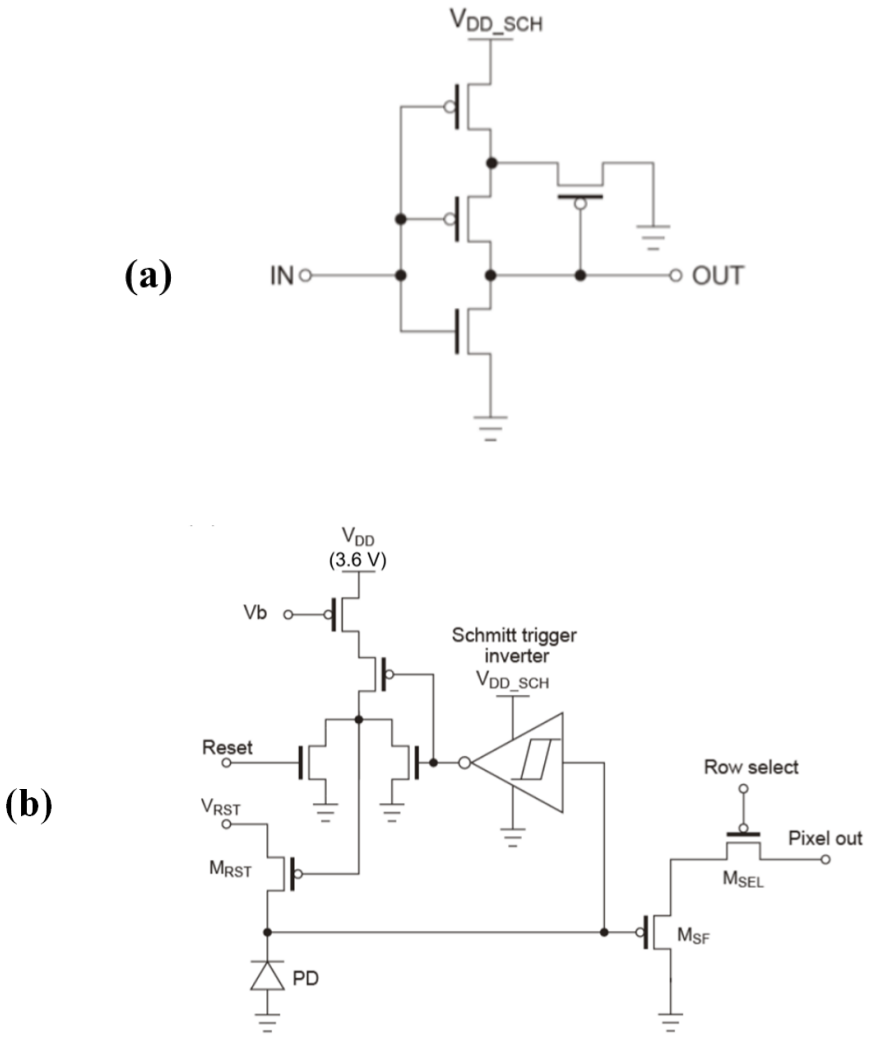

Figure 23 (a) circuits of Schmitt trigger inverter, which consists of 3 p-channel transistors and an n-channel transistor and (b) Self-reset pixel [46]**.**

The pixel output cannot be fixed due to the hysteresis characteristics. As a result, a reliable self-resetting operation is achieved. Our prior pixel also employed this architecture, and the self-resetting circuit worked perfectly. However, as the PD voltage falls below or near the threshold, the Schmitt trigger inverter's power consumption rises. This effect causes the pixel to heat up, increasing noise and can cause the chip to malfunction. Thus, reducing power consumption is required. One of our goals is to develop an implantable self-resetting image sensor, so the pixel size should be maintained. As a result, the Schmitt trigger inverter's power consumption was lowered by operating it at a low voltage in the later generation. The power supply line is independent of the rest of the pixel and can be regulated separately. The number of transistors and the size of the circuit are the same as in our previous pixel. We can lower the gate-source voltages of the transistors by lowering the supply voltage. As a result, low current consumption is attained.

2.6.1 Self-reset pixel

A pixel circuit design is shown in **Figure 23(b)**. The pixel contains eleven transistors. The output circuit's source follower (SF) is made up of p-channel transistors. This is because the threshold voltage of self-resetting is reduced by reducing the supply voltage for the Schmitt trigger inverter. However, the Schmitt trigger inverter in our self-resetting is made of p-channel transistors. As a result, the additional area penalty associated with utilizing a p-channel transistor is negligible. The row select switch is also made up of a p-channel transistor, which lets the full signal from the p-channel SF pass through.

2.6.2 The previous generation self-reset image sensor and Characteristics

The image sensor specifications of the previous version are shown in Table II. The standard 0.35-μm 2-poly-4-metal CMOS process was used. The Schmitt trigger inverter's supply voltage is

1.7 V, while the other circuit's supply voltage is 3.6 V. The pixel dimensions are 15 by 15 meters. The fill percentage is 29%.

Table II Specification of the previous generation self-reset image sensor

Technology	0.35-μm 2-poly 4-metal standard CMOS process
Chip size	1.1 × 3.0 mm
Pixel size	15 × 15 μm^2
Photodiodes	n-well / p-sub
Fill factor	29 %
Operating voltage	3.6 V

In terms of noises, the principal temporal noise sources in an image sensor are the readout circuit's thermal noise T, pixel reset noise (RST), and photon shot noise (SN). Photon shot noise is proportional to the square root of the number of photoelectrons in this case. Other sounds, such as 1/f noise and random telegraph noise, can be ignored in high-intensity applications since they are relatively weak. Noises observed in self-reset image sensors will be examined further.

We evaluated the characteristics of the fabricated pixel. An array of green LEDs with an emission peak of 525 nm was used as a light source. A diffusion plate was used to obtain uniform illumination. The bias voltage V_b and the reset voltage V_{rst} were set to 2.6 and 2.0 V, respectively. The frame rate was set to 11.25 frames per second. **Figure 24(a)** shows the signal output as a function of the irradiated light power. The vertical axis is the sensor output. The output was reconstructed by adding a product of the pixel output amplitude and a number of self-resets. The raw data shows a saw-tooth curve. However, the reconstructed data is proportional to the light power. Here, the nonlinearity of the sensor output was also compensated for in the measured result.

As shown in **Figure 24(b)** shows the noise level, which is the standard deviation of the sensor output as a function of light intensity. The pixel array's median value is displayed. In areas with low light intensity, it is practically flat. The readout and pixel reset noises determine the noise floor in this case. Because this sensor lacks a noise reduction circuit such as correlated double sampling, the noise level is relatively high compared to standard four-transistor active pixel sensors. The noise level rises in proportion to the incident light intensity and is proportional to the square root of it. Thus, the photon shot noise is dominant in this region. However, compare to the typical image sensor noise component from **Figure 11**, the self-resetting process generates additional noise after the first resetting is triggered due to the resetting, which it could cause an unstable stage. At an intensity of 2.310×10^{-6} W/cm^2, the first self-resetting occurs. On average, self-resetting adds about 1.5 dB to the noise level in this case. On the other hand, the noise level is dependent on light output and varies from pixel to pixel.

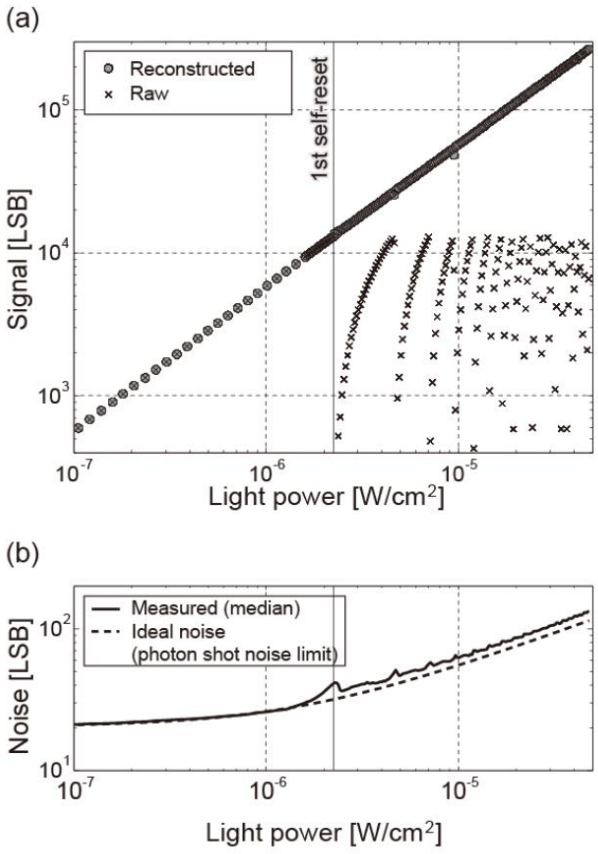

Figure 24 (a) Signal and (b) noise intensity as functions of incident light power. The wavelength of the irradiated light is 525 nm [46]**.**

2.6.3 In-vivo imaging with the previous generation self-resetting image sensor

Previously, our group succeeded in performing in-vivo imaging with a self-resetting image sensor. For detecting local conversion between oxyhemoglobin (HbO) and deoxyhemoglobin (HbR) in brain tissues, a self-resetting image sensor and orange light-emitting diodes (LEDs; λ= 605 nm) were included in an implantable imaging device. We exhibited imaging of hemodynamic responses in the sensory cortex region of a living mouse in response to forelimb stimulation. The implantable imaging device for intrinsic signal detection is anticipated to be a potent tool for

analyzing the behavior of living animals by measuring brain activity. The device implanting the self-resetting image sensor for this hemodynamic response is shown in **Figure 25**.

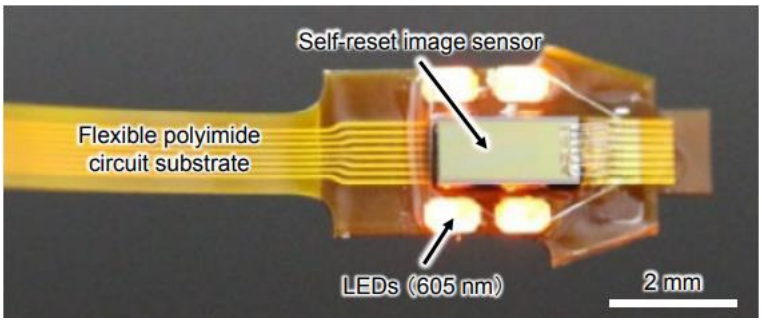

Figure 25 The in-vivo imaging device made for Hemodynamic response imaging.

The result of this hemodynamic response imaging is shown in **Figure 26** [7].

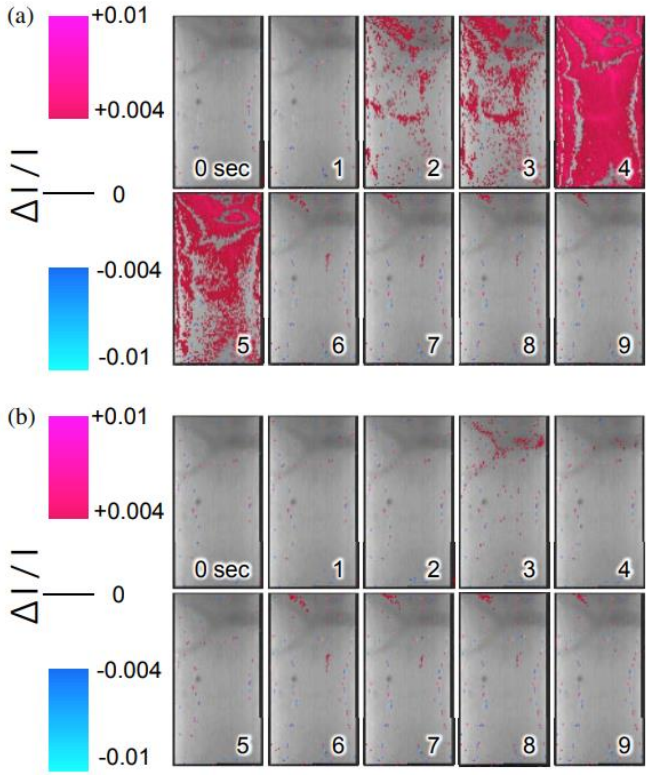

Figure 26 *in-vivo* imaging result of the hemodynamic response by stimulating the hindlimb of the mouse. (a) shows a result of the right front limb. (b) shows the result from the hindlimb [7]**.**

More than that, the self-resetting image sensor also succeeded in implementing 2-color imaging.

The experiment diagram is shown in **Figure 27**. The captured image is shown in **Figure 28**.

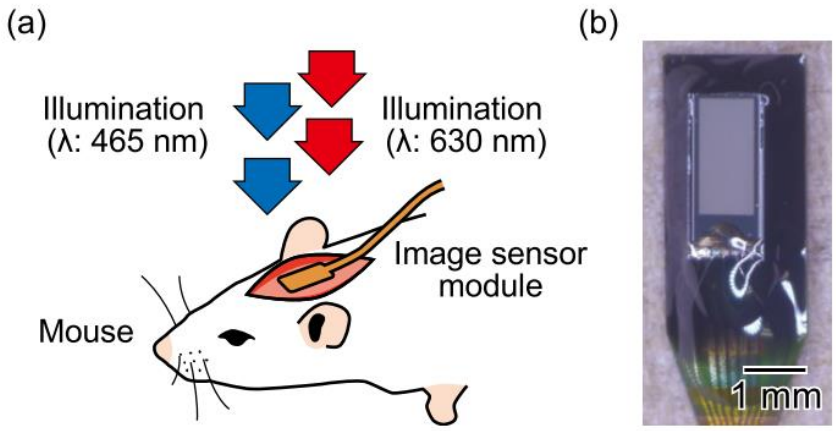

Figure 27 (a) Graphic shows an experiment set-up. (b) micrograph of the self-reset imaging device in this experiment [46]**.**

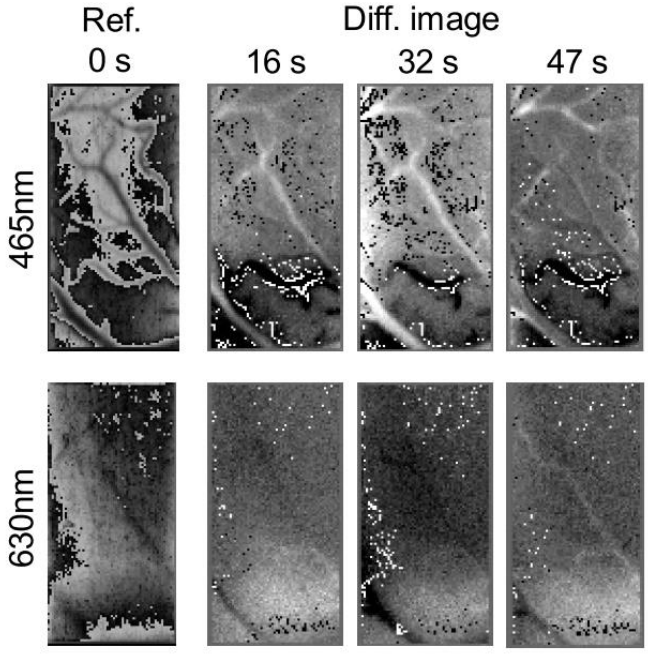

Figure 28 Images captured in time lapse from the 2-color imaging [46]**.**

The upper and lower rows are images for the wavelengths of 465 nm (blue) and 630 nm (red), respectively. High-contrast boundaries resulting from self-resets were observed. At 465 nm, the blood vessels were visible because of the high optical absorption by hemoglobin. The differential images show the difference in intensity from the reference images. The black or white spots resulted from the change in the number of self-resets. They can be reduced by estimating and correcting the self-reset number. After the stimulation, continuous intensity changes were observed for each wavelength. The correlation of the intensity changes between the two wavelengths was not high. This suggests that the results include blood density and the ratio of HbO to HbR.

2.7 Discussion

Research points out clearly that monitoring neural activity from the living brain is necessary for studying the neural circuit and its complicated function. Various approaches have been developed for this function, such as electrophysiology and optical imaging. However, when it comes to requiring a high definition of the observing part, it turns out that optical imaging methods have better capabilities than electrophysiology. In many cases, electrophysiology keeps suffering from high noise and other artifacts. Furthermore, an unbearable limitation is the inability to record the specific neurons. Therefore, optical imaging is a worthwhile and significant innovation.

According to the literature, extrinsic signal optical imaging, such as calcium imaging or green fluorescence, is far more practical for moving free-moving animals. Maybe this is the outcome of the advanced and more complicated preparation needed for green fluorescence imaging. So far, many devices have been developed for the task. Those existing devices mainly rely on a commercial part for an imaging module designed for multipurpose and adaptability. The

majority of these devices still use the miniaturized-microscope concept. Therefore, the device must be in combination with the lens. Though the lens provides a high definition in imaging, it comes with equal weight in a trade-off, which is the weight and size of the device. Because the optical system must be considered when designing the device housing.

Along with the advancement of green fluorescence imaging, intrinsic optical signal imaging also proves its strong advantage over green fluorescence imaging because it can be performed without genetic engineering in preparation and has a good capability of imaging cerebral blood flow. This could have advantages regarding multi-wavelength imaging for calibration in green fluorescence imaging. However, it was discovered that the measurement equipment and devices still need to be developed since most of the measurements so far are still in head-fixed mouse experiments. How potent could intrinsic signal imaging be incorporated into the head-mounted device or implanted in combination with any other technique? Therefore, an intrinsic signal image was chosen to be made into a small device at this time.

Among the various imaging methods, it has one outstanding feature that suits the application the most. It is contact imaging. With the lensless image sensor, it has the potential to be utilized to develop an imaging device that is implantable despite its extremely small size and light weight. According to the image sensor, which can work without a lens, the device design and packaging size can be drastically decreased. Despite some of the constraints, the numerous design and techniques that have been discussed so far can be integrated and truly make this a functional device easily.

The challenging issues in CMOS image sensors are both dynamic range and SNR. Despite the earlier work that had been done to expand the dynamic range, it was discovered that one method could be useful for in-vivo brain imaging. It is the self-reset technique that can improve dynamic

range and SNR at the same time. This technique overcomes the parameter that caps the SNR directly, which is the limitation of FWC. Utilizing this technique, it could be integrated at a pixel level under the capabilities of the CMOS standard process. Normally, the existing self-reset image sensor did not design for *in-vivo* imaging and mainly aimed to expand the dynamic range.

The existing self-reset image sensor from the other group was created mainly to expand the dynamic range. Fortunately, this technique recycles the FWC as if the pixel could handle the flooded electrons. This mechanic overcomes the limitation that caps the peak SNR, which is the limitation of FWC. Consequently, this method simultaneously increases both the DR and SNR. Consequently, applying this method could also benefit in-vivo imaging since the image sensor for this specific application requires an extremely high SNR. In addition, a high DR is a positive trait that can be advantageous in certain circumstances.

Since in-vivo imaging is quite a unique function, the existing device might not be suitable for this application due to its physical properties and spatial resolution. To realize a pixel with a self-reset function, the circuit for the self-reset trigger must be included in the pixel. And for acquiring images, a reset counting circuit might be necessary for the image reconstruction. All of these related circuits were built-in for good image reconstruction, but the trade-off was an excess pixel size. For the self-resetting trigger circuit, a comparator is a common choice for detecting the photocurrent level and triggering the self-resetting. For these reasons, it results in a very low fill factor even with the excess pixel size. The fill factor is quite important for contact imaging, which always suffers from light diffraction and also depends on the illuminating strategy in the experiment setup. Thus, the pixel will get a burden as it needs to make the most of the photons that have been delivered.

Previously, our group presented the self-resetting image sensor. Our implantable image sensor devices have no lenses and are used by contacting the samples directly. The self-reset function was realized by the 4-transistor Schmitt trigger inverter, which utilized 3 p-channel transistors and 1 n-channel transistor. This circuit functions as a simple comparator to detect when the voltage of the parasitic capacitor of the photodiode is getting lower than the threshold of the inverter. Then, the self-reset would be triggered. In the first generation of self-resetting image sensors, it was discovered that the power consumption of the Schmitt trigger increased as the photodiode voltage decreased and approached the threshold.

Consequently, it caused both power consumption and thermal issues. Therefore, it is necessary to separate the power supply line from the rest of the circuit to be independently controlled. Accordingly, the Schmitt trigger was operated freely with low voltage. Thermal and power consumption issues were resolved. Resultantly, the self-reset pixel circuit appears in figure 22. The operating voltage for this Schmitt trigger has been optimized to 1.7 V.

The self-reset image sensor from our group needs no reset counting circuit since our target signal is the very small change of the light intensity between frames. Thus, this subtraction image was acquired by subtracting each frame from the reference frame. So, the small changes in these values would be emphasized as an intrinsic signal. Accordingly, the reset cycle number is unnecessary. However, the number of reset cycles could be approximated by counting the image data acquired at low light intensity. Under these conditions, our self-resetting pixel could be so small that it could be manufactured using the standard 0.35-μm CMOS process. The comparison between those existing self-reset image sensors and the latest self-reset image sensor from our group [7] is shown in Table III. Since the advantages of our self-resetting image sensor is to detect

the small changes brain signal in each frame with high SNR, the comparison would be focused on the effective SNR, pixel size, and fill factor which is directly related to the application.

Table III Comparison of the existing self-reset image sensor

	[47]	[48]	[40]	[49]	[7]
Technology (μm)	0.25	0.35	0.18	0.50	**0.35**
Tr./pixel	N/A	N/A	43	28	**10**
Pixel size (μm^2)	45 × 45	25 × 25	19 × 19	49 × 49	**15 × 15**
Self-reset type	Comparator	Comparator	Comparator	Schmitt trigger	**Schmitt trigger**
Counter	8-bit	1-bit	6-bit	6-bit	**-**
Fill factor	23%	27%	50%	25%	**31%**
Maximum frame rate	1 kHz	15 kHz	1 kHz	> 1 kHz	**300 Hz**
Peak SNR	N/A	74.5 dB	55.6 dB	65 dB	**59 dB**

This image sensor was designed for high light intensity operation to achieve a high SNR. Therefore, the noise that typically affects the signal within the region of low light intensity can be disregarded. Only the dominant noise in the region of high light intensity should be considered. Theoretically, the only dominant noise at high light intensity is the photon shot noise.

Even if the self-reset function for obtaining high SNR has been accomplished and refined to resist the shot-noise limit, this self-reset image sensor has the potential for even greater efficiency. Depending on the self-resetting downtime, it may generate an unstable stage during operation, particularly at high resetting frequencies. Therefore, it is preferable to lower the number of reset cycles in order to achieve a more stable operation and eliminate the system's artifacts. Moreover, it was discovered that after the initial reset, as depicted in **Figure 29**, the SNR decreases

and forms a new offset for the remainder of the process. This issue should be resolved to enhance imaging performance.

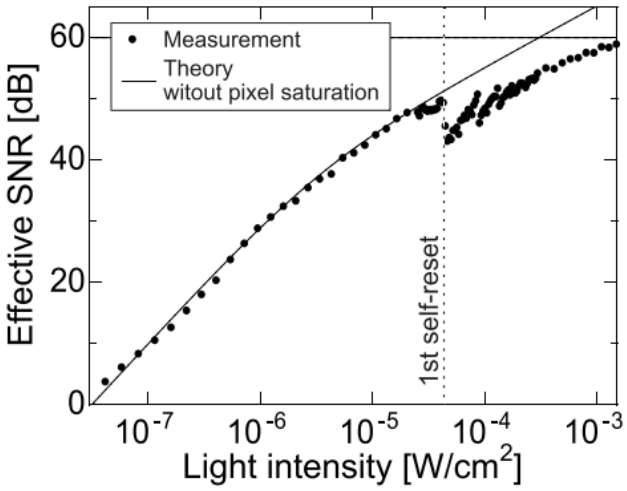

Figure 29 SNR characteristic of the previous self-reset image sensor shows the SNR drop after the self-resetting was triggered [46]**.**

2.8 Summary

To push forward in-vivo imaging, there still needs to be a lot of advancement in imaging devices. It was discovered that each optical imaging method also needs different conditions and approaches. Thus, it was found that the existing device design for green fluorescence imaging, such as calcium imaging, is by far more practical and closer to completely free-moving animals. Moreover, within such a complicated organism like the brain, every method has its limitations. So, for the next step of in-vivo imaging, multi-wavelength or double device imaging is required for learning more complicated neuronal activities. Intrinsic signal imaging is one method of advantage in imaging cerebral blood flow. It could be used to learn many kinds of activities and be combined with other methods to enhance its purpose. Thus, a more advanced imaging device for intrinsic signal imaging is needed. In addition, from this study, it was found that the device of the future

will not only be able to image its target neuron but also size or possess the capabilities to work in combination with other methods, including small size, light weight, wide dynamic range, and high SNR.

Using the self-reset method, our group developed a self-resetting image sensor for in-vivo imaging in order to achieve such a promising device. A 0.35-μm CMOS standard process was used to fabricate the chip. Through numerous enhancements, the pixel size has remained at 15×15 μm^2 to preserve an adequate spatial resolution for the unique purpose. The self-resetting pixel does not require the reset counting circuit since the image acquisition method detects minor light intensity changes between frames by subtracting the image. The peak SNR reaches over 60 dB. However, there are ways to improve the image sensor, as it has been found that self-resetting causes downtime and an unstable stage. Thus, reducing the number of self-resetting cycles should reduce the artifact introduced by the resetting system. To solve the SNR-drop after triggering the self-resetting also needs inspection.

Chapter 3 Self-resetting image sensor utilizing the modified structure photodiode method and MOS capacitor method

An outstanding performance of the image sensor is required to identify changes in intrinsic brain signals of roughly 0.1 percent. A high SNR of greater than 60 dB is necessary to monitor these small signals. In prior work, we proposed a self-resetting pixel to produce a highly effective SNR. We reached an SNR of 64 dB, which allowed us to detect the hemodynamic signal from the mouse brain while also stimulating it. The experiment, however, can yet be improved. If the device's effective SNR is high enough, it has a chance of receiving a better high-definition signal from the brain. We discovered that the active circuit connected to the V_{rst} is unstable, which could result in a signal drop, or a 3 dB increase in noise during the initial reset. It then serves as a floor for the entire SNR after triggering the first self-reset. This voltage loss must be minimized to improve the efficiency of this imaging device.

This time, two methods were demonstrated for improving this self-reset CMOS image sensor. The first method uses a modified photodiode structure to enhance photodiode capacity and attain even better effective SNR. P-diff/N-well/P-sub structure was chosen as a photodiode because its physical structure offers a greater thin layer area than N-well/P-sub at the same size, resulting in a better capacity. The pixel will be able to handle more electrons in a single resetting cycle. In other words, it minimizes the amount of self-resetting cycles and avoids the unstable period. At this time, we also employed a new relay board with improved performance. We also

developed an image processing to decrease artifacts caused by the self-resetting mechanism. **Figure 30** shows the device implementation concept.

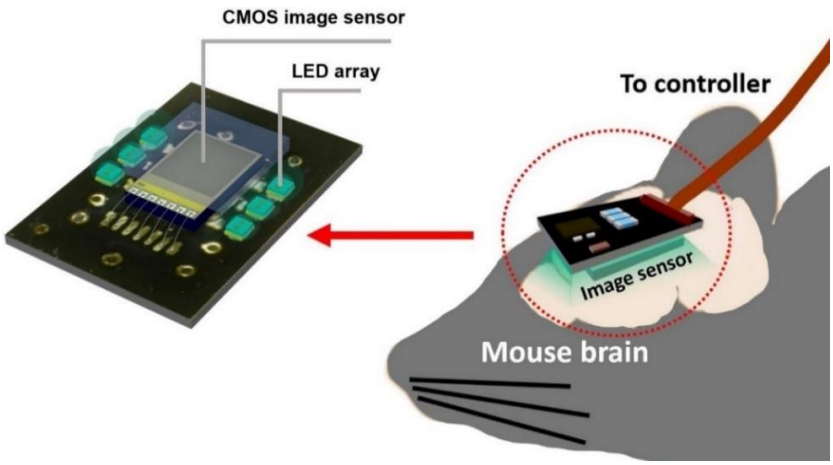

Figure 30 A self-reset implanted image sensor for sensing an inherent signal from a hemodynamic reaction is shown. The proposed image sensor was mounted on the relay board, which was encircled by LEDs.

3.1 *The principle of self-resetting image sensor*

Self-resetting image sensors detect the level charge amount in the capacity and reset it before saturation. As a result, the effective pixel capacity and the amount of light that can be processed can be enhanced. High dynamic range imaging is one benefit of its applications. Our goal, however, is to achieve a high effective SNR. Photon shot noise is the dominating other noise factors when the light intensity is very strong. Its value is proportional to the square root of the incident light signal. The keys to realizing a high SNR are avoiding pixel saturation and handling many photon charges. We must first establish the parameter limiting the effective SNR before discussing high SNR in the self-resetting sensor. The photon shot noise is the predominant noise under high-intensity conditions. The total noise of the self-reset sensor $\sigma_{SELFRST}$ is approximate,

$$\sigma_{SELFRST} \simeq \sigma_{SN}\sqrt{\frac{\sigma_{RST}^2}{FWC}+1} \qquad (1)$$

σ_{RST} is the pixel reset noise, σ_{SN} is the Photon shot noise, and FWC is the FWC of the pixel. In the case of sufficiently high FWC, the total noise asymptotically approaches σ_{SN}. Then, the signal components are shown as equation (2).

$$V_{sig} = V_{out} + N \cdot A_{out} \qquad (2)$$

From equation (2), V_{sig} is the reconstructed pixel output, V_{out} is the pixel output, N is the number of resetting cycles, and A_{out} is the maximum amplitude of the pixel. The effective SNR is described as equation (3).

$$SNR_{eff} = V_{sig}/\sigma_{SELFRST} \qquad (3)$$

We discovered that the SNR of the self-reset sensor is about the same as a typical image sensor under high light intensity conditions using equations (1) and (3). The V_{sig} can go as high as proportional to the light intensity because the self-resetting technology prevents the pixel from becoming saturated. After the signal reconstruction post-process, the intensity signal can be obtained by compensating for an estimated number of resetting cycles. The effective high dynamic range is one of the benefits of self-resetting pixels. However, in this study, we concentrated on detecting tiny signals with a high SNR, such as the changing intrinsic brain signal. Therefore, the number of self-resetting required for reconstructing the pixel output is not required in this demonstration because the target signal is the very small intensity that changes in each frame,

obtained by subtracting the reference frame from each frame of raw data, not the normal image or real light intensity.

3.2 Self-reset pixel with modified photodiode structure

3.2.1 Pixel circuit

The prior version's circuit design is still in use. The 4-transistor Schmitt trigger inverter from the previous generation is still used. In order to save electricity, it is powered by a lower voltage (VDD2) than the other components. **Figure 31** shows the pixel circuit with the Schmitt trigger inverter included.

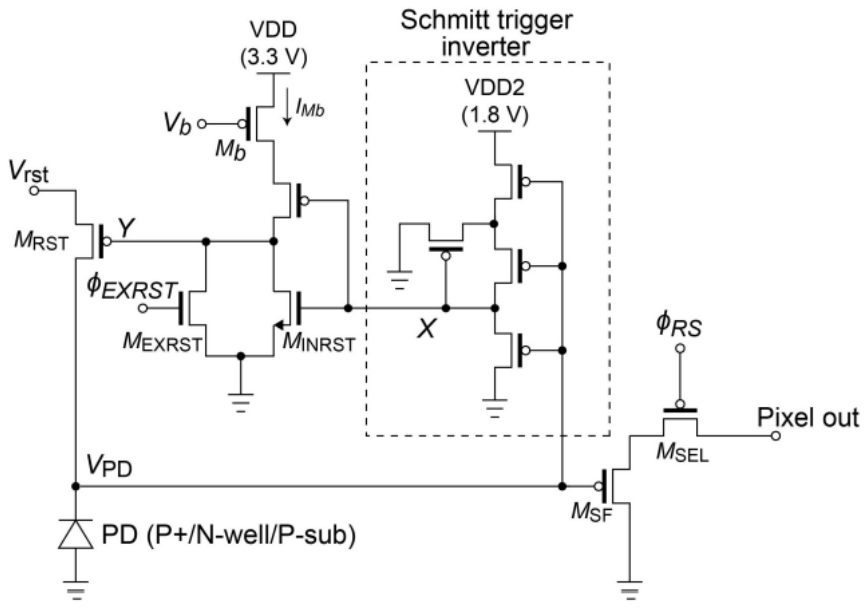

Figure 31 The schematic of the self-reset pixel with a low-voltage driven Schmitt trigger inverter. The PD is composed of P+/N-well/P-sub.

The type of photodiode used in this study was P+/N-well/P-sub. Compared to the normal n-well/p-sub arrangement, commonly used in 3-transistor APS pixels, this structure enhances the photodiode's capacitance. The pixel size, however, remains constant at 15 × 15 μm^2. The pixel

contains 11 transistors, which is the bare minimum for this method. **Figure 32** illustrates the suggested pixel with a photodiode arrangement.

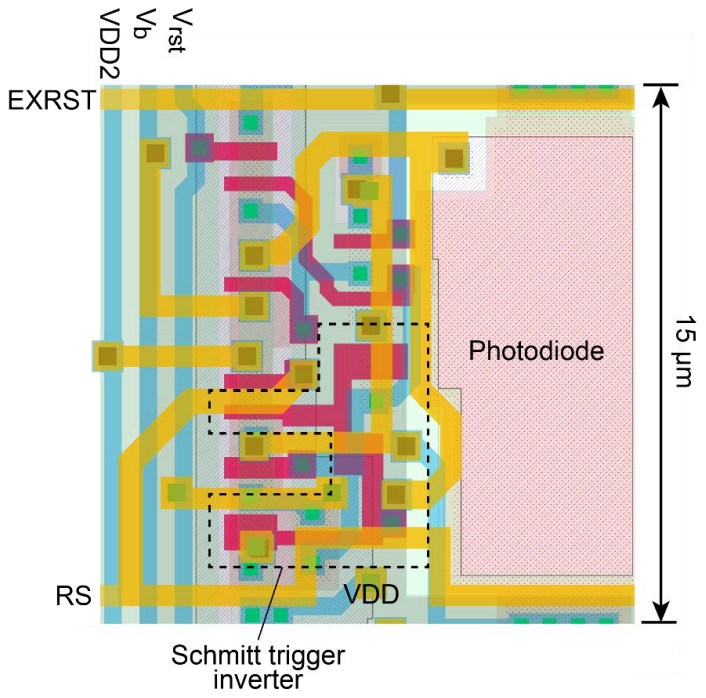

Figure 32 Layout of the pixel with P+/N-well/P-sub photodiode.

3.2.2 Pixel simulation

The pixel circuit operation was simulated. VDD1, VDD2, and V_b were set to 2.4, 2.5, and 1.8 V, respectively. In addition, to imitate the photocurrent to the PD, a 1 nA constant current source was put in parallel with the PD. **Figure 33** shows the results that self-resets occur many times. The photocurrent gradually lowers the V_{PD} once the PD is charged to the reset voltage (V_{rst}) by an external reset. The node X in **Figure 31** is inverted and becomes HIGH when it decreases to the threshold of the Schmitt trigger inverter.

Furthermore, the inverter circuit inverts the signal, and the reset signal of node Y becomes LOW. This LOW state has a duration of roughly 100 nanoseconds. During this time, no optical

signal may be detected. The output change during this interval is $1/1.67\times10^4$ of the voltage swing of VPD when the frame rate is 30 fps, and the number of self-resets is 20 times per frame. The SNR reaches 70 dB in this situation. Because the photon shot noise, the dominating temporary noise, is expected to be around $1/3\times10^3$, the self-reset time in this situation is sufficient.

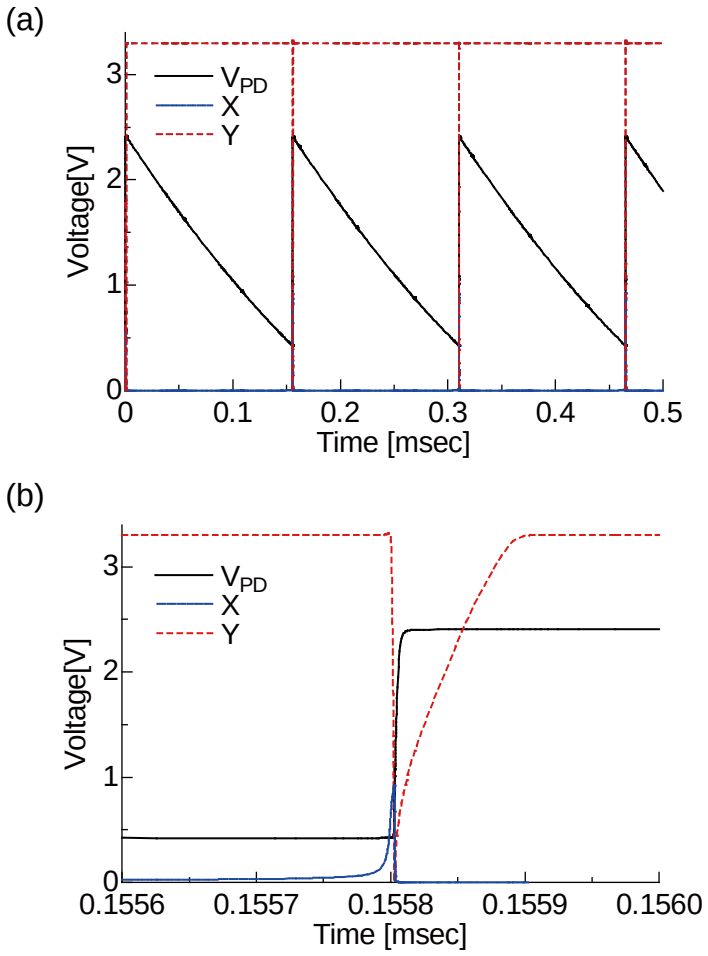

Figure 33 Simulation results of the self-resetting pixel. (b) is the magnified plot of the self-resetting region. X, Y correspond to the nodes indicated in Figure 31.

3.2.3 Image sensor chip and specification

Figure 34 shows an image of the created chip. The 0.35-μm 2-poly 4-metal standard CMOS process was used. Table IV shows the specifications. There are 128×128 pixels in all. The

basic structure of this image sensor is the same as our implantable image sensor, with the control line decreased by using an external clock to provide a control signal. On the other hand, the analog signal line is brought in from the outside. As a result, seven signal lines exist. During self-reset, the V_{rst} drops significantly. However, this must be reduced. Installing a sufficient performance bias inside the chip is tough. An analog voltage signal is output from the picture sensor.

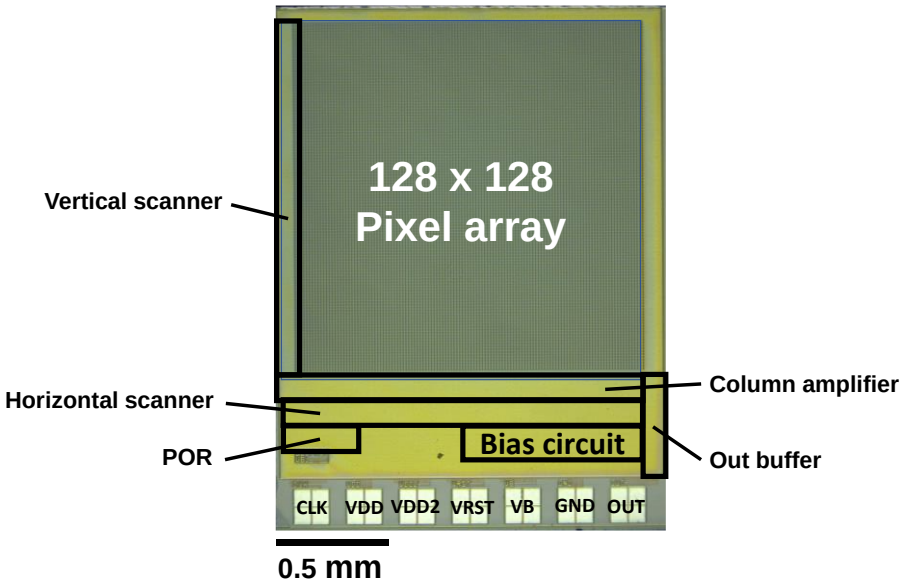

Figure 34 Photograph of the proposed image sensor with 128 × 128 pixel array.

Table IV Specifications of the chip

Technology	0.35-μm 2-poly 4-metal standard CMOS process
Chip size	2.7 × 2.1 mm^2
Pixel size	15 × 15 μm^2
FWC enhancing	P+/N-well/P-sub
Fill factor	30 %
Pixel number	128 × 128
Operating voltage	3.3 V
Pixel type	3-Tr active pixel sensor with 4-Tr

3.3 Imaging module with a self-reset image sensor

This custom printed circuit board (PCB) was designed and fabricated to connect the image sensor and the data processing board. Since the output of the image sensor is an analog signal, it is equipped with a preamplifier circuit. As mentioned in the previous section, V_{rst} must be stable. It is required to minimize the amplitude and duration of the voltage drop due to self-reset. Since it is difficult to obtain a sufficient response speed in an active circuit, passive noise filters (NFM18PC, Murata) have been inserted into the V_{rst} line on this board. On the other side, the image sensor and six LEDs were mounted, as shown in **Figure 35**.

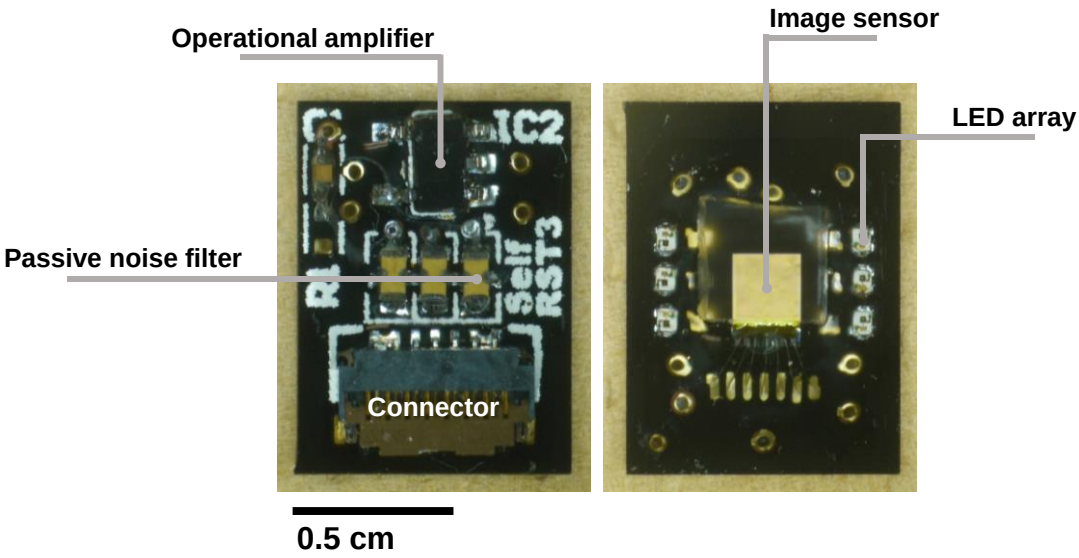

Figure 35 The finished device ready for the application.

Figure 35 shows the photos of the relay board (left), the preamplifier circuit, and the passive noise filters. (Right) The image sensor is positioned at the center of the PCB, between the LED arrays to take advantage of the high light intensity. We chose bluish-green surface mounted diode LED with a center wavelength of 530 nm (SMLP13EC8TT86, ROHM). The image sensor surface was waterproofed by covering it with a fiber optic plate and sealing it with epoxy glue.

Because the intended use is to implant into the mouse brain, we must consider the heat conditions and the waterproof packing. After connecting the electrodes with aluminum wires, epoxy was utilized to preserve all of the electrode surfaces. An artifact is caused by a light incident from the side of the picture sensor. To prevent this, a black color resist was used between the LEDs and the sensor. A fiber optic plate covers the image sensor itself (FOP, J5734, Hamamatsu). The FOP is an optical device comprised of a network of micro-optical fibers. It transmits an image incident on its input surface directly to its output surface. The thickness of the chip was 500 μm. This FOP protects the image sensor surface and maintains a safe distance between the brain surface and the mounted LED, as heat can cause damage.

3.4 Imaging Device characteristics

3.4.1 Pixel Output

Based on the pixel circuit shown in **Figure 31**, V_b can control the current that runs through the p-channel transistor M_b. Thus, the self-resetting time can be changed. The voltage was set to 2.5 V with a reset time of about 0.1 μsec.

The chip was illuminated by a homogeneous beam with a peak emission wavelength of 530 nm in this measurement. The test was carried out at room temperature. The output signal as a function of the light intensity is shown in **Figure 36**. The self-resetting is activated when the pixel voltage V_{PD} displayed in **Figure 31** falls below the threshold of the Schmitt trigger inverter. As a result, the output signal is reset to zero. As a result, the output has the shape of a saw tooth. When the number of self-resetting is known, the true lit signal may be easily reconstructed. The reconstructed signal output is also presented in **Figure 36**. The output amplitude and an estimated number of self-resetting were added to the signal for reconstruction. As a result, the prototype

device has light intensity nonlinearity, and the slope change is significant, particularly just before and after self-reset. As a result, in the imaging experiment using this device, a look-up table was created based on this finding, and image processing was used to rectify the image.

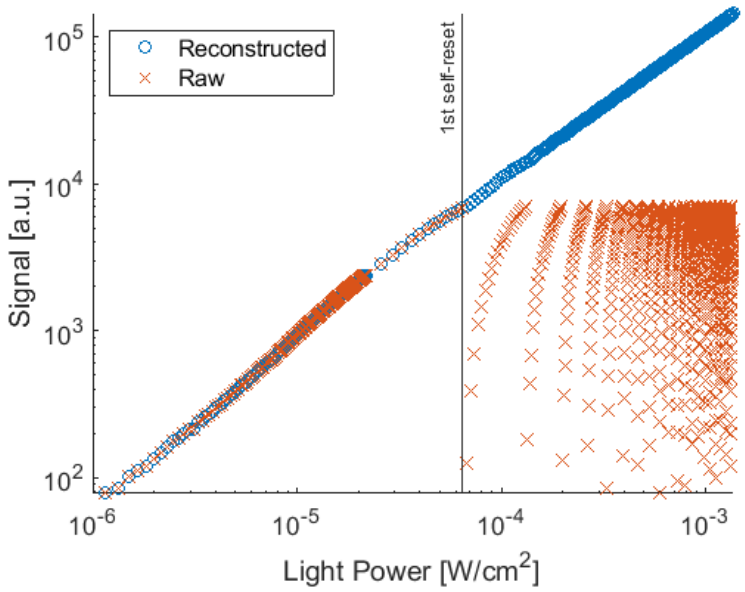

Figure 36 The signal from the pixel with P+/N-well/P-sub photodiode as a function of the light intensity.

Figure 37 depicts the effective SNR versus light output. It was calculated using Eq (3). Figure 37 shows the results of the prior n-well/p-sub structure (a) and the p +/n-well/p-sub structure (b). The plot points with low SNR appear at the boundary of the self-resets in the high light intensity zone. It can be decreased by self-resetting and fixing the artifacts. A typical noise curve was fitted to get the solid line. **Figure 37** indicate that SNR increases by order of magnitude in low illuminance by 20 dB and 10 dB in high illuminance. This is compatible with the fact that in low illuminance, noise independent of light intensity, such as external resetting and pixel readout, is dominant. In high illuminance, on the other hand, photon shot noise dominates. The SNR was increased using the noise filter described in the following section, resulting in a highly effective SNR of 70 dB or higher in both pixels.

The older version has a lower capacity due to the changed photodiode construction. As a result, it has a greater SNR in low light than the new pixel. This area, however, is unimportant for our objectives. In the high illuminance range, however, the effective SNR is roughly the same. Because of the limited photodiode capacity, the device self-resets more frequently and enters an unstable state. Particularly, the noise grows due to self-resetting dead time and the residual error of response nonlinearity. These problems can be rectified by reducing the number of resets. At a light intensity of 1.35 mW/cm^2, the n-well/p-sub structure had 52 times of self-resetting and the p-diff/n-well/p-sub structure had 21 times. Regarding the period of self-resetting, the ratio of PD capacitances in the previous and current sensors is roughly 1:2.6. As a result, the total effective SNR is nearly the same, but the current design has resulted in a more stable device.

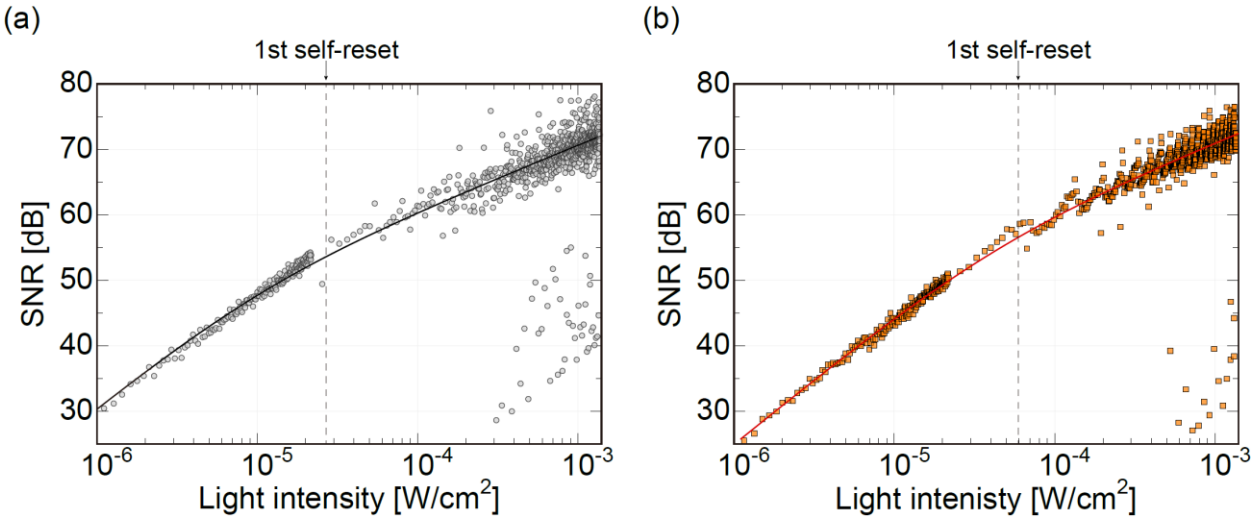

Figure 37 (a) SNR of the pixel with N-well/P-sub photodiode, (b) SNR the pixel with P+/N-well/P-sub photodiode.

3.4.2 Performance Improvement by the Relay Board

In a prior study, the noise increased dramatically after the first self-reset was triggered due to some factor that kept lowering the total effective SNR, as shown in **Figure 29**. It was hypothesized that this was due to the reset potential briefly dropping and the V_{rst} potential not returning to a constant value until the self-reset process was completed. Thus, it causes an additional unstable state and is included in the noise from the self-resetting system. The new relay board was developed for this issue by introducing a noise filter (NFM18PS, Murata) on the V_{rst} line. This is to support the self-resetting procedure and ensure that the V_{rst} can be fully retrieved at the ending of each self-resetting procedure. The result from implementing this new relay board compared to the previous version is shown in **Figure 38**.

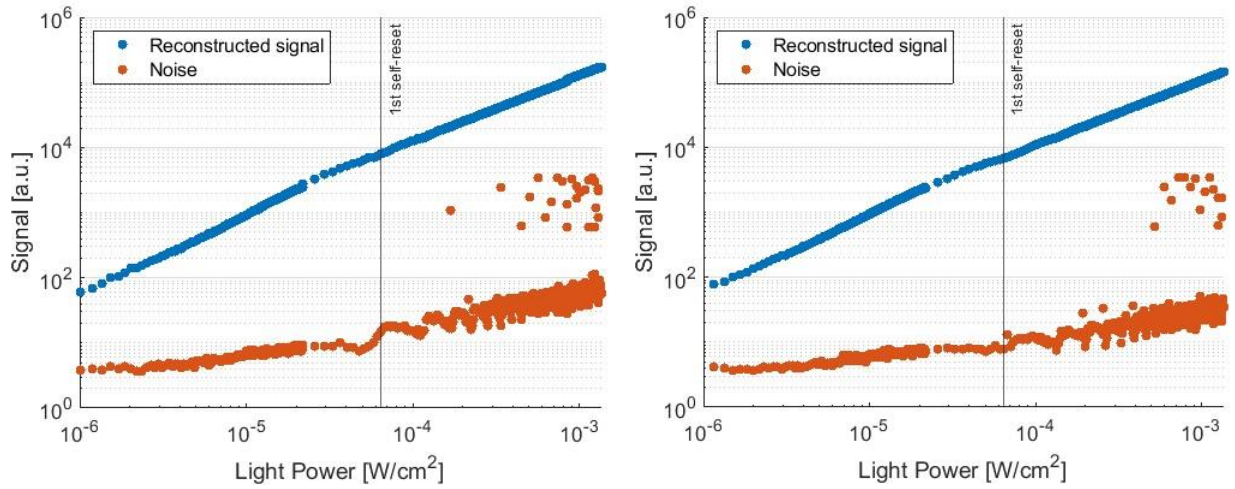

Figure 38 shows the reconstructed data and noise of the self-reset pixel comparing between (a) using the previous version of PCB and (b) using the latest version of PCB introducing the noise filter.

The noise is increasing due to the photon shot noise which is the dominant noise in this region. Refer to the noise in typical image sensor from the **Figure 11**. In the case of a self-resetting image sensor, the self-resetting appears to be an additional noise source since the self-resetting

causes an unstable state. Thus, providing a more stable operation could reduce the noise and realize a higher SNR. Figure 39 shows the noise comparison between the previous version of the relay board and the latest version, which uses a noise filter. The result has it that the noise was reduced drastically. Therefore, the SNR is improved.

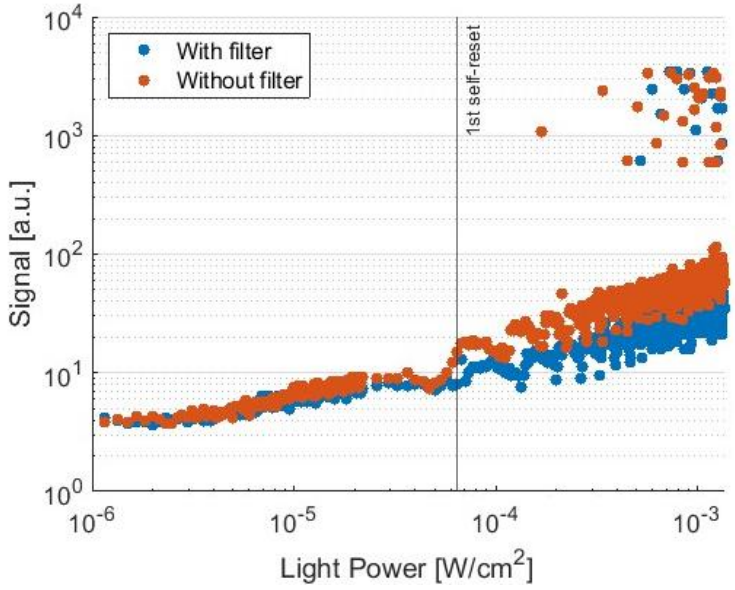

Figure 39 Noise level as function of light power comparing between relay board with and without noise filter.

The difference in effective SNR with and without a filter is shown in **Figure 40**. The data from the filter-equipped device is also used in the result that is seen in **Figure 37**. The dashed line is the curve that was fitted to the data without the filter. Only the offset from the fitted curve for the device with the filter has been modified in this case.

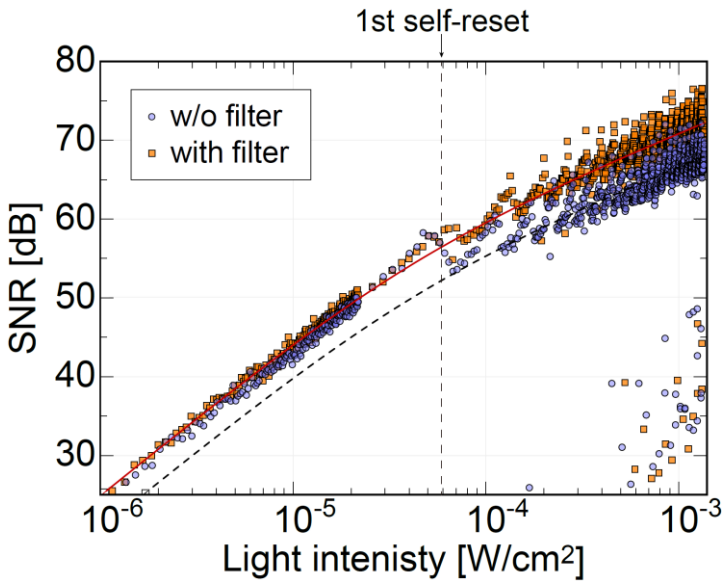

Figure 40 Effective SNR as a function of incoming light intensity between image sensors employing relay boards with and without a noise filter on the V_{rst} line.

As with previous devices, there was a considerable SNR loss on the initial self-reset without the filter. The filter, on the other hand, did not cause a noticeable rise in noise. As a result, we achieved an SNR improvement of roughly 4 dB. To decrease noise, we used a passive filter. According to the simulation results, the self-reset process should take no more than 0.1 nsec. That means a response bandwidth of at least 10 GHz is necessary. Low power and active electronics make accomplishing such a fast response challenging. Stable operation is achieved by attaching an external filter with a capacity sufficiently greater than the pixel capacity and rapidly charging the PD capacity in the pixel. The results reveal that our latest relay board has minimized the SNR-dropping behavior during the first self-resetting. The later result within this thesis is the data from the device that equipped the new relay board.

3.5 Self-resetting image sensor pixel with Metal-Oxide-Semiconductor (MOS) capacitor

One method for enhancing the FWC is using a MOS capacitor. Another version of the self-reset image sensor will be presented. In terms of increasing the FWC, introducing an additional capacitor into the photodetector node is a straightforward idea of the concept. This additional capacitor can be realized using a MOS capacitor. According to the low-voltage driven Schmitt trigger, it has less penalty to use the p-channel transistor as a MOS-capacitor for this time.

3.5.1 MOS capacitor

The MOS capacitor is normally a two-terminal device consisting of three layers: a metal gate electrode, a separating insulator, which usually is an oxide layer, and a silicon substrate or body. The MOS capacitor structure diagram is shown in **Figure 41**. The MOS capacitor that was used in this study was realized by introducing a p-channel transistor to directly connect to the photodiode. The source and drain of the transistor are connected to the VDD to realize the structure as shown in **Figure 41**. The connecting regulation is shown in **Figure 42** within the next section. The gate was connected to the V_{PD}, the body of the transistor was connected to the VDD. This MOS capacitor will work in depletion mode.

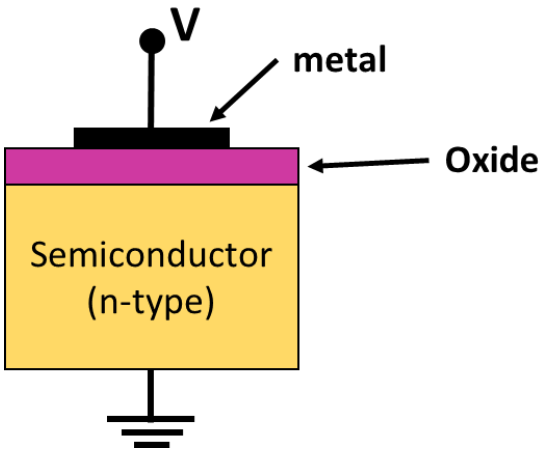

Figure 41 shows a typical p-channel MOS capacitor structure.

According to minority charge was the main role in this mode. It can't maintain high capacitance at high frequency since those minority charges can't follow the changes of the signal at high frequency. However, intrinsic signal imaging of the brain's activities does not require such a high frame rate. The frame rate of this image sensor is set to 15 fps. Thus, it is low enough to maintain the performance of the MOS capacitor.

3.5.2 Pixel circuit

The circuit of this version is quite similar to the pixel with the modified photodiode. However, N-well/P-sub photodiode was used instead. The PMOS-capacitor was inserted at the photodetector node. The schematic of this version is shown in **Figure 42**. The pixel layout is shown in **Figure 43**.

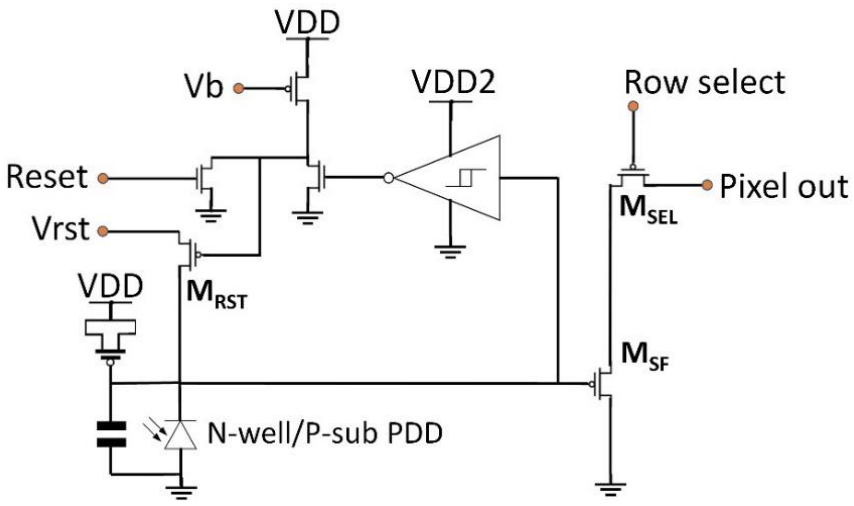

Figure 42 The schematic of self-reset pixel with MOS-capacitor. The body of the p-channel MOS capacitor was connected to the VDD, while the gate was connected to the PD node.

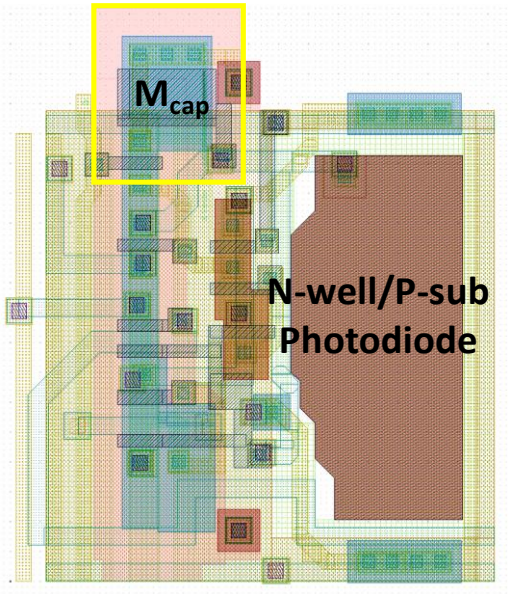

Figure 43 Layout of the self-reset pixel with MOS-capacitor (M_{cap}).

The MOS capacitor seems to take extra space until it stays out of the pixel frame, as seen in **Figure 43**. However, the MOS capacitor was well designed to take place in the free space of the next pixel. Thus, the pixel size and chip dimensions are not changed. An array of these pixels is shown in **Figure 44**. The MOS capacitor could take up some space in the neighboring pixel. The pixel pitch is not changed.

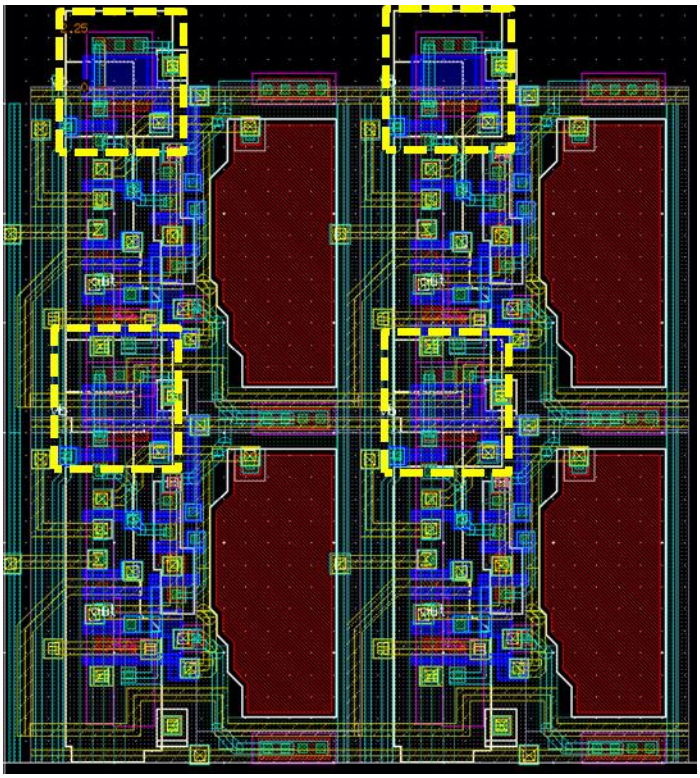

Figure 44 Array of the pixel with MOS capacitor, which is managed to overlap into neighboring pixel for maintaining the pixel pitch.

3.5.3 Image sensor chip and specification

As mentioned, the pixel size and chip dimension are not changed, but the overall chip appearance stays the same, as shown in figure 32. All of the related parts or relay board can be used the same as the other version. The specification is listed in Table V.

Table V Specifications of the chip

Technology	0.35-μm 2-poly 4-metal standard CMOS process
Chip size	2.7 × 2.1 mm^2
Pixel size	15 × 15 μm^2
FWC enhancing	MOS capacitor
Fill factor	30%
Pixel number	128 × 128
Operating voltage	3.3 V
Pixel type	3-Tr active pixel sensor with 4-Tr Schmitt trigger inverter for self-resetting

3.5.4 Performance Improvement by introducing MOS capacitor

For this version, the input parameter is the same setup as the modified photodiode version. Through the evaluation, the pixel output is shown in **Figure 45**. It was found that this version has moderate FWC compared to the pixel using a modified photodetector according to the self-reset function was triggered at lower light intensity. The resetting cycle numbers are also higher at the same light intensity. Thus, FWC could be estimated.

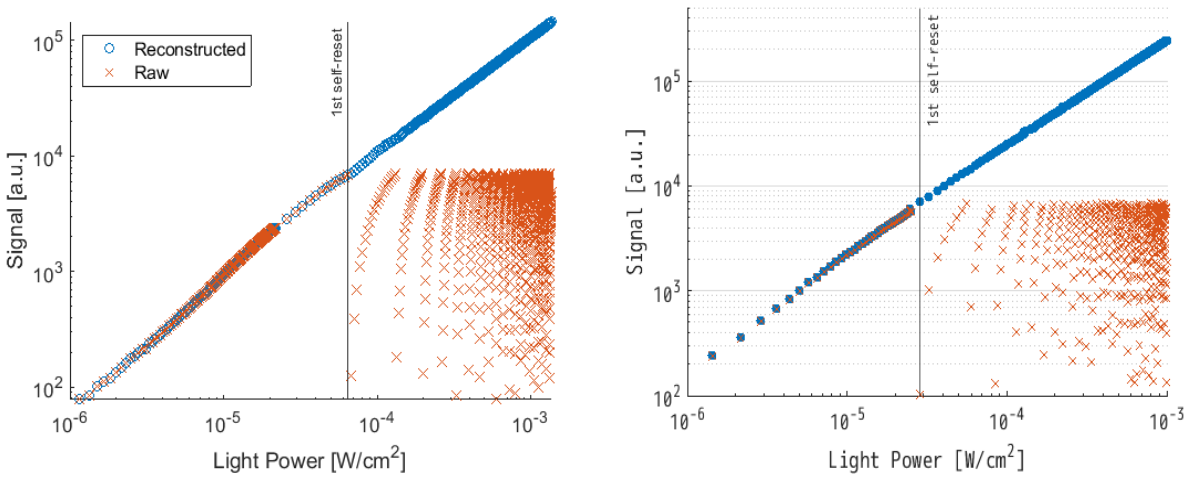

Figure 45 Evaluation result from both version of the pixel. (Left) The pixel with modified photodiode structure (Right) The pixel with MOS-capacitor.

Though this version has a smaller FWC, it has been seen clearly that the pixel with MOS capacitor offers better linearity from the plot in **Figure 45**. In given the fact that the capacitive characteristics of the photodiode mostly influence the linearity, it was discovered that an extremely large FWC results in a slight decrease in linearity, as seen by an evaluation. This linearity can be evaluated through the R-squared value of the pixel within the range of intensity before the self-resetting is triggered. To compare the linearity of these two image sensors, the sample of pixels was selected from the center of the image sensor for 225 pixels. The result is shown in figure 46. This graph is plotted from the R-squared of the raw data within the range of intensity before the self-resetting would be triggered.

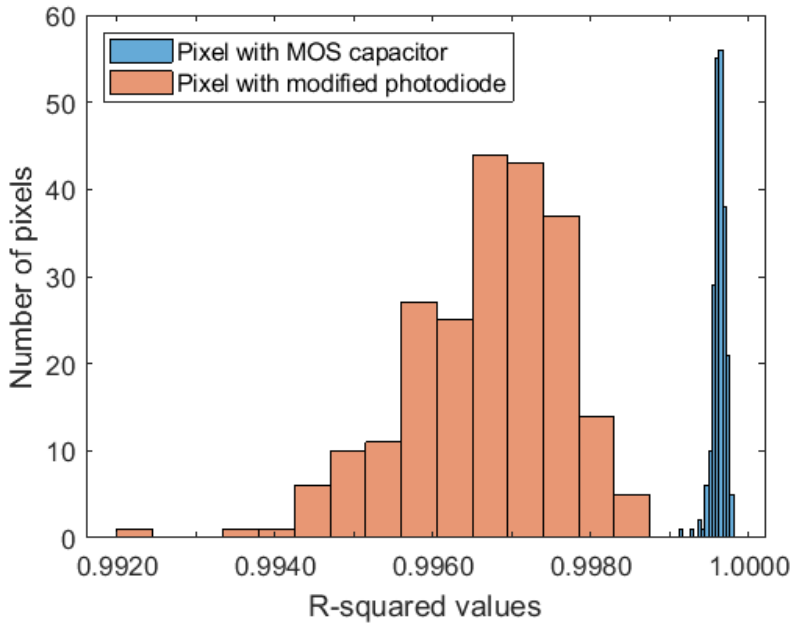

Figure 46 Histogram shows linearity through the R-squared values of the 225 selected pixels at the center of both versions of the image sensor.

The linearity in the low light intensity region is affected by various sources, including readout noise and also the capacitive characteristics of the photodiode. From the figure 46, it was found that the pixel with MOS capacitor offer a lot better linearity compared to the pixel with modified photodiode. And even though the FWC of the pixel with MOS capacitor is not extremely large, it could provide an identical high SNR as the pixel with the modified photodiode. The SNR evaluation result is shown in **Figure 47**. The pixel with the MOS capacitor has a smaller FWC, as indicated by the first self-resetting was triggered at a lower intensity than the pixel with the modified photodiode.

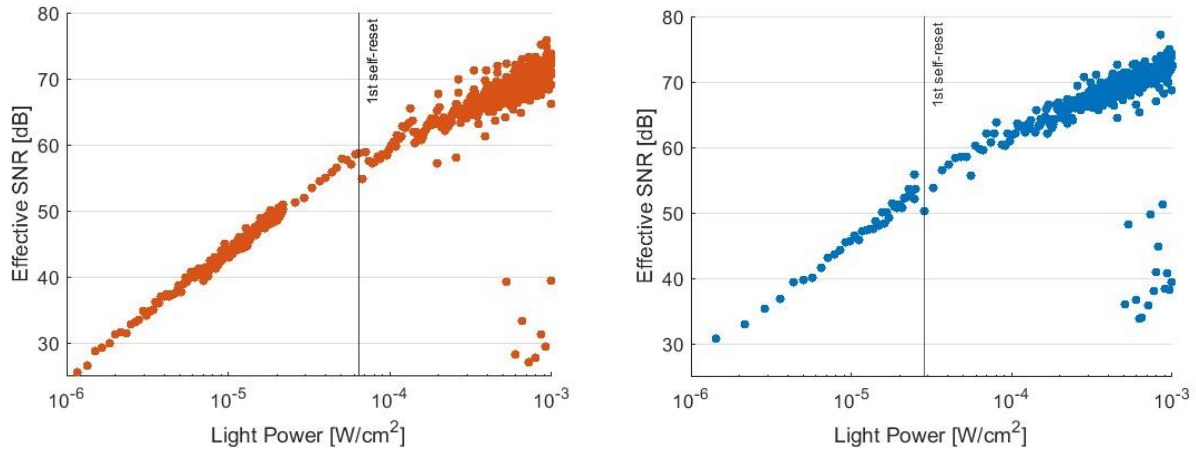

Figure 47 (Left) SNR of the pixel with N-well/P-sub photodiode, (Right) SNR the pixel with MOS capacitor.

3.6 Discussion

3.6.1 The improvements of self-resetting image sensor

From the evaluation result, it was found that enlarging the FWC obviously improves the self-resetting operation by reducing the resetting cycles since it reduces the fluctuating data and probability to appear as a resetting boundary after the image processing. However, the relative performance of these two variants of the image sensor is different. It was found that the self-reset pixel with a modified photodiode structure has a two-times larger FWC than the pixel with a MOS-capacitor due to its physical structure and properties. Hence, it has lower light sensitivity and also a better performance at reducing the self-resetting cycles. On the other hand, though the pixel with MOS-capacitor has a smaller FWC in comparison, it still has a moderate FWC for the function. At the same time, it offers better linearity, which is very important for image acquisition. As a result, the pixel with a MOS-capacitor appears to be the most compromising candidate for future generations. However, the limitation of the pixel with the MOS-capacitor is the operating frequency due to the electrical properties.

In combination with the new relay board, the low SNR offset after the self-resetting was initiated was solved. Therefore, the in-vivo imaging device implementing the new image sensor has better performance.

3.6.2 Comparison with Other Sensors in the Previous Works

The proposed pixel is modest and small yet has a high fill factor. The SNR is up to 64 dB for the previous prototype [7]. This time, we increased the SNR to over 70 dB using the modified photodiode structure or MOS capacitor while keeping the other parameters, such as pixel size and fill factor, stay the same as optimized for the application. Furthermore, the larger FWC technique provides a more stable operation. Because a higher FWC minimizes the number of self-resetting, the unstable stage could be avoided. It was outstanding compared to the existing device regarding the unique in-vivo imaging application. Because the pixel has a small circuit, we can achieve a higher fill factor at a finer fabrication than other self-reset pixels. The proposed image sensor was developed to track the activity of the brain. As a result, the great dynamic range is less significant than the small intensity change, which is the target signal. Thus, what is important is that the SNR is high enough to detect small changes in brain activity.

Furthermore, the fill factor is an important parameter to detect illumination effectively because it allows you to avoid utilizing too much light intensity to complete the task, which can raise the temperature and harm the brain. In addition, without using a self-resetting counter circuit, this proposed image-acquiring technique has the probability of broadening the variety of applications.

3.6.3 Limitations of pixel performance

In terms of frame rate, based on the simulation presented in **Figure 33**, the self-reset down time along the resetting process can be ignored since this application does not require such a high frame rate. However, the self-resetting duration should be shorter for applications that need a high SNR and a high frame rate, such as voltage-sensitive dye imaging, which requires a frame rate of around 1 kHz or more. Thus, the frame rate of the current design is not enough. Even if V_b is adjusted to reduce the self-reset time, the simulation indicates that V_{PD} will not be reset securely until it touches the V_{rst} level properly. To accomplish high-speed functioning, modifications such as increasing the size of the reset transistor are required.

3.7 Summary

Both versions of the self-reset pixel were improved to reach over 70 dB. The pixel with a modified photodiode has a larger FWC, lower light sensitivity, and drastically reduced self-resetting cycles, but it has poor linearity. Though the nonlinearity could be fixed by calibration with the pixel characteristic measured in advance, it could still be a problem if the brightness changes significantly. On the other hand, the pixel with MOS-capacitor has a smaller FWC. Thus, it has higher sensitivity and is moderately effective at reducing the self-resetting cycles. However, it offers better linearity. Hence, it performs better if handling high contrast imaging is needed. The limitation of this pixel is the operation frequency since the capacitance of the MOS capacitor will be affected.

Chapter 4 In-vivo imaging and Image processing

4.1 Experimental setup

The inherent signal was observed at the mouse brain surface for the imaging demonstration. We used the C57BL/6JJmsSlc wild-type mouse from Japan SLC, Inc. The barrel cortex, a sub-region of the somatosensory cortex, is the target area. It is in charge of the mouse whisker, which will be used for physical stimulation. The experiment setup diagram is depicted in **Figure 48**. The mouse was anesthetized, and the stereotaxic device was used to stabilize and fix it. The imaging device was positioned on the target location of the brain's surface. We went with bluish green with a 527 nm central wavelength (SMLP13EC8TT86, ROHM). This time, the mouse we utilized was a wild type. All animal experiment operations were conducted under Nara Institute of Science and Technology's animal care and experimental rules.

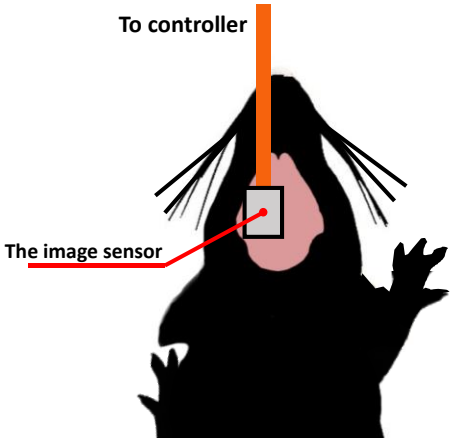

Figure 48 The imaging equipment was put in the somatosensory cortex area on the left side of the brain, while stimulation was done on the opposite side.

The image sensor was mounted on the latest version of the relay board and tested with the built-in LED. **Figure 49(Left)** depicts a device with a turn-on LED. The image sensor was

concealed and was visible through the FOP. The mouse brain surface was prepared as shown in **Figure 49(Right)**. The dura was removed. Thus, the blood vessel on the brain surface was shown clearly and easily for the imaging alignment. As suggested in **Figure 50**, the device was aligned on the brain surface, targeting the somatosensory cortex.

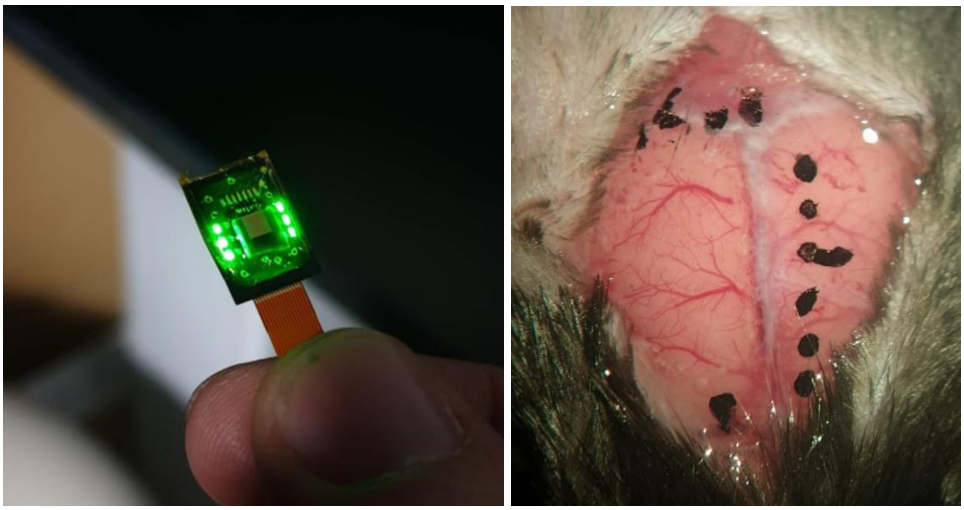

Figure 49 (Left) The imaging device with the built-in LED turned on. (Right) Mouse brain surface with roughly scale for locating the somatosensory cortex.

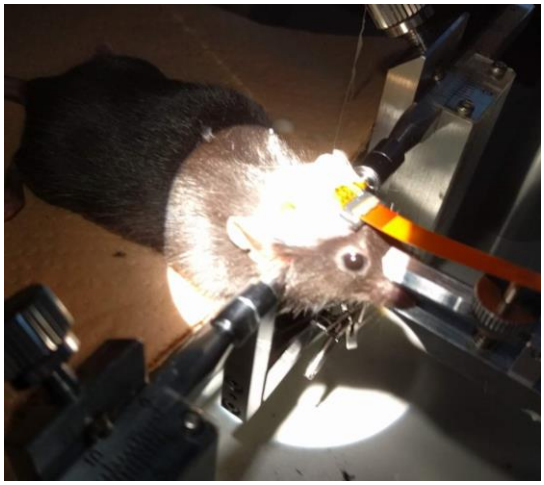

Figure 50 The device was perfectly aligned to the brain surface.

As depicted in **Figure 51**, the raw image could be viewed through the user interface of the custom program called ‘CIS-NAIST’, in order to verify the alignment. Despite the absence of a reset counting circuit, this program's interface allows for a rough count of the reset number.

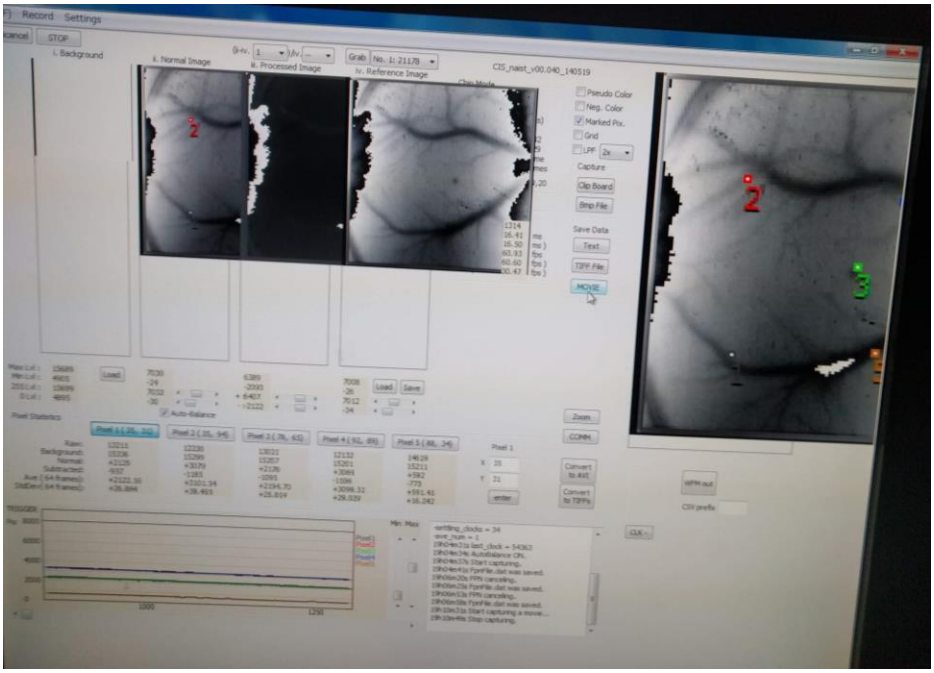

Figure 51 CIS-NAIST user interface for the alignment and observing the mouse brain.

Since this image sensor is designed to work at a very high light intensity, the image data needs post-processing to analyze the brain surface signal. The image processing will be described in the next part.

4.2 Image processing and Imaging results

Since the self-reset function is integrated into each pixel, the pixel can reset itself freely or whenever the voltage level drops down to the threshold. When taking an image, it usually consists of the different light intensity between each area. Therefore, the area with a high light intensity will trigger the self-reset function first before the pixel in the darker area where the voltage level is not yet touching the threshold. Thus, leave the boundary like an onion ring called "Resetting boundary," as shown in **Figure 52**. The self-reset image sensor takes this image in combination with a lens to show the self-resetting that occurs along the surface with different light intensities.

Figure 52 An image taken by the self-reset image sensor using a lens to show the resetting boundary along the surface with different light intensity.

The photographs of the mouse brain are shown in **Figure 53**. **Figure 53(a)** shows a photograph taken using a microscope. The yellow square indicates the location of the image sensor. A raw output image is shown in **Figure 53(b)**. A frame rate of 15 frames per second was used. The imager resets itself when the light intensity hits the threshold. As a result, the image shows the fringe pattern of the folded intensity. This is not a problem for our purpose, which is to examine

the intensity change from a reference image. The effective SNR is crucial for detecting minor intensity variations in the intrinsic signal. The normal image can also be reconstructed using a reference image or an estimation technique. **Figure 53(c)** depicts the rebuilt image.

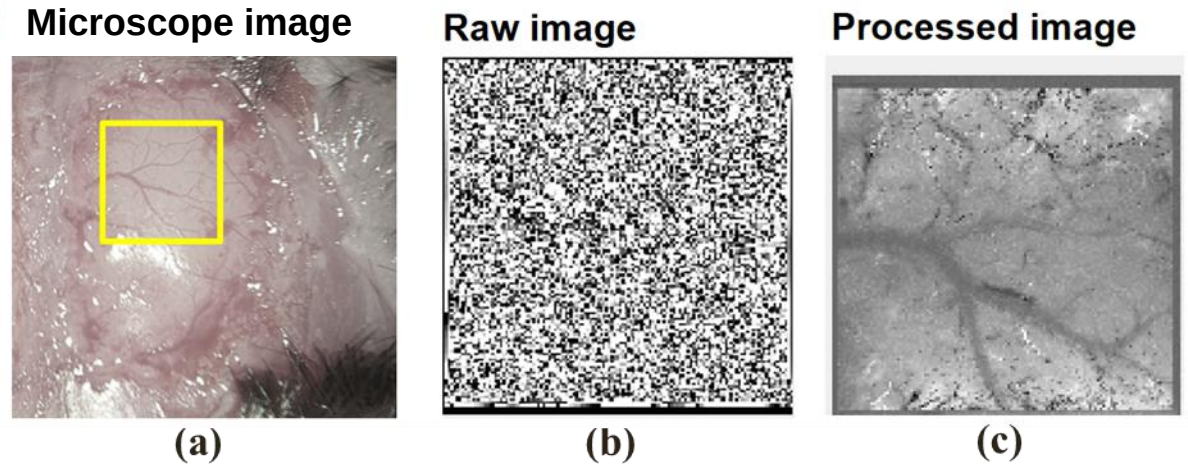

Figure 53 The brain surface with the target area, raw image, and post-process image.

4.3 Image Reconstruction

4.3.1 Correction of folding artifacts by self-resetting

An example of raw imaging is shown in **Figure 54**. The pixel output becomes a folded waveform due to self-reset as shown in **Figure 55(a)**. Generally, a mechanism for counting the number of resets is required to restore an image. However, it is not always necessary to irradiate light and observe weak changes, as is the purpose of this research. The amount of irradiation light can be controlled, and the amount of change in the signal observed from the immediately preceding frame is small. If only the relative amount of change is observed, counting the number of self-resets is not necessary. In addition, if the intensity of the light source is gradually increased during measurement, the number of self-resets can be confirmed by tracing the history.

The observation target was a living mouse, and an imaging device was placed on its brain surface. The image is one frame at the observed light intensity. It is a folded image at the boundary between self-reset and the number of times. **Figure 55(a)** is a graph showing the signal strength change at a boundary point. It can be seen that when the intensity gradually changes and exceeds the threshold value, the number of resets changes, and the output fluctuates greatly. In intrinsic imaging on the brain surface, it can be assumed that extremely large fluctuations do not occur. It means that large fluctuations are changes in the number of resets. The result of setting the threshold value and removing the artifact is shown in **Figure 55(b)**. In this result, there are still artifacts left. Residual artifacts occur because they had intermediate values during self-setting. There are two possibilities for the intermediate values. The first is the case that the change is smaller than the threshold, although the pixel was self-reset. The second is the case where the value is intermediate but exceeds the threshold value and is counted twice.

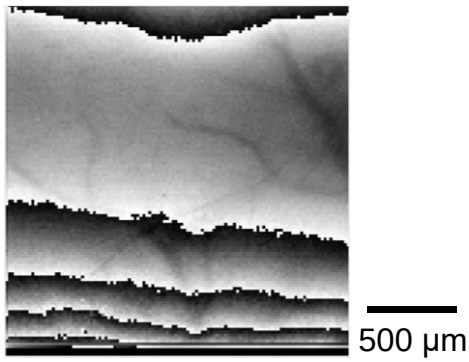

Figure 54 Raw image of the brain surface acquired by the self-reset sensor.

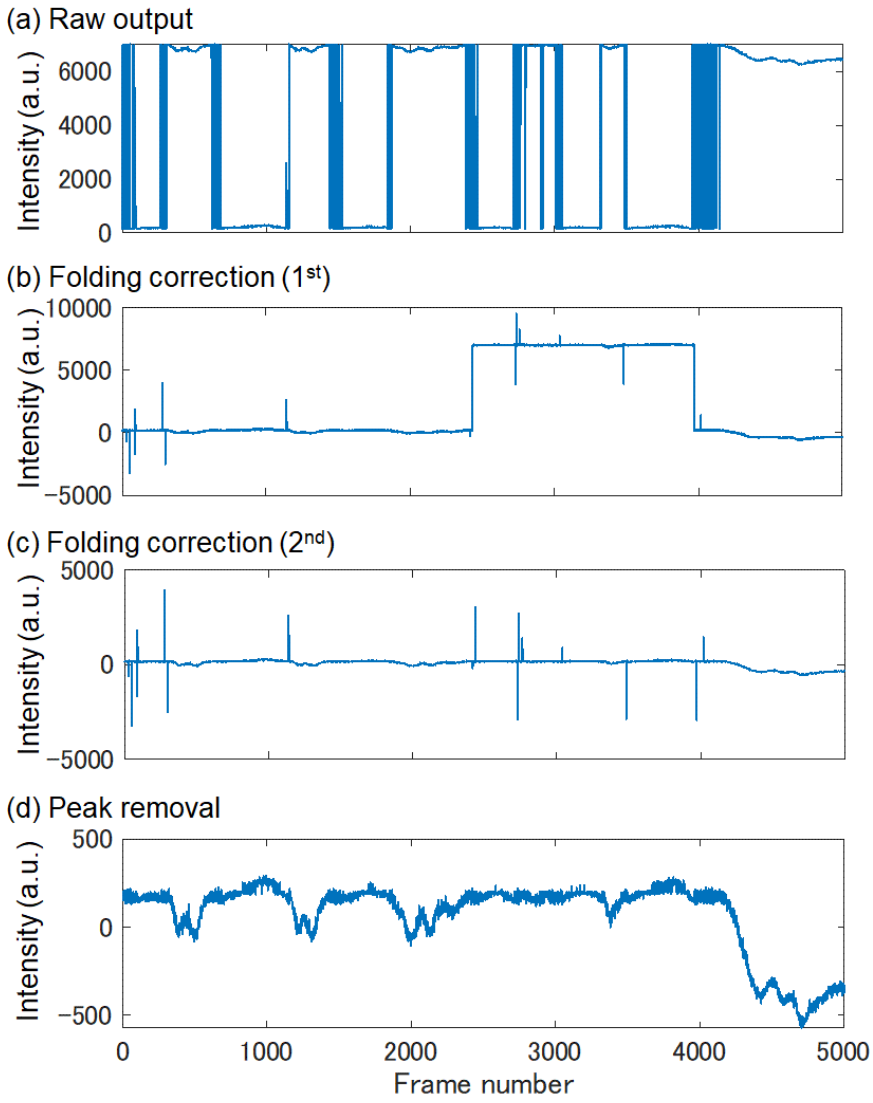

Figure 55 Correction of artifacts by self-resetting.

In order to deal with this, the correction is made based on the frames up to two frames before. The result is shown in **Figure 55(c)**. Improvements can also be seen for artifacts that could not be detected the first time. Finally, strong peaks were removed, as shown in **Figure 55(d)**.

When reconstructing, it is necessary to add the maximum amplitude of the pixel multiplied by the number of self-reset times. However, there are variations in MOSFET characteristics. If the maximum amplitude is constant over the entire imaging region, an artifact will occur in which the output fluctuation near the reset boundary becomes large. In order to reduce this, the maximum and minimum values of each pixel were acquired from the frame of the measurement data, and the corrected values were used.

4.4 Nonlinearity correction

As shown in **Figure 45**, there is pixel output nonlinearity. Nonlinearity was also present in intra-pixel photodiodes with a simple n-well/p-sub structure, which is difficult to remove completely. In this design, the p+/n-well/p-sub structure is used to increase the pixel capacitance per area, but this increases the capacitance change due to voltage and further increases the nonlinearity. The amount of change in output with respect to light intensity gradually changes with the output voltage, but the point where the output becomes the maximum value and the point where it becomes the minimum value are connected by the correction of folding by the self-reset sensor. Therefore, a very large difference can be seen near the boundary of the number of resets.

The nonlinearity is greatly influenced by the capacitive characteristics of the photodiode and is then given by the source follower of the readout circuit. To correct this, we prepared a look-up table (LUT) that linearizes the output from the image sensor output as a function of irradiation

light intensity data. The relation of output versus input is plotted in **Figure 56**. Here, for the nonlinear correction, the same one was used for the entire pixel array.

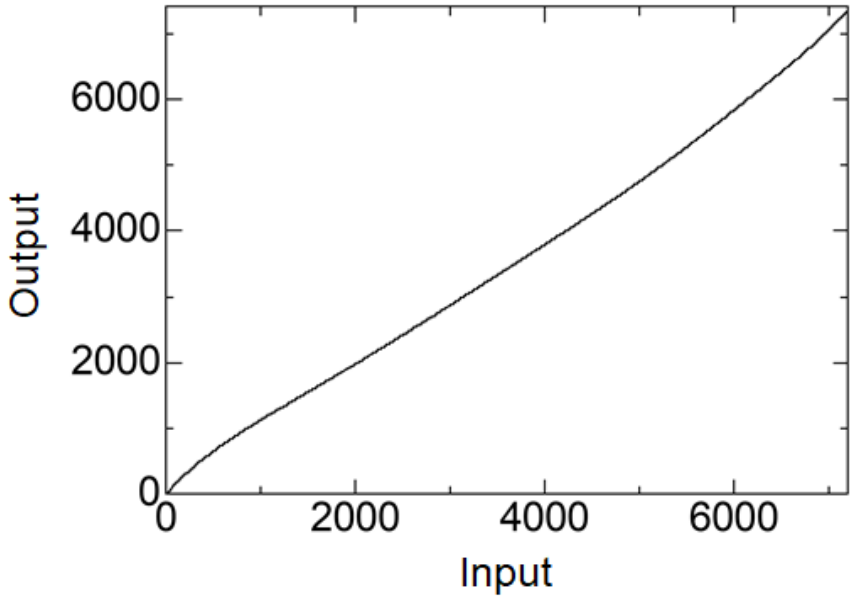

Figure 56 Output versus input of the look up table for pixel nonlinearity correction.

Figure 57 shows a line scan of the blood vessel. The dark streaks show the migration of red blood cells. by plotting the brightness change in the blood vessel over time. Blood flow in the blood vessels causes a diagonal pattern to appear. Blood flow velocity was measured at 1.4-2.8 mm/sec.

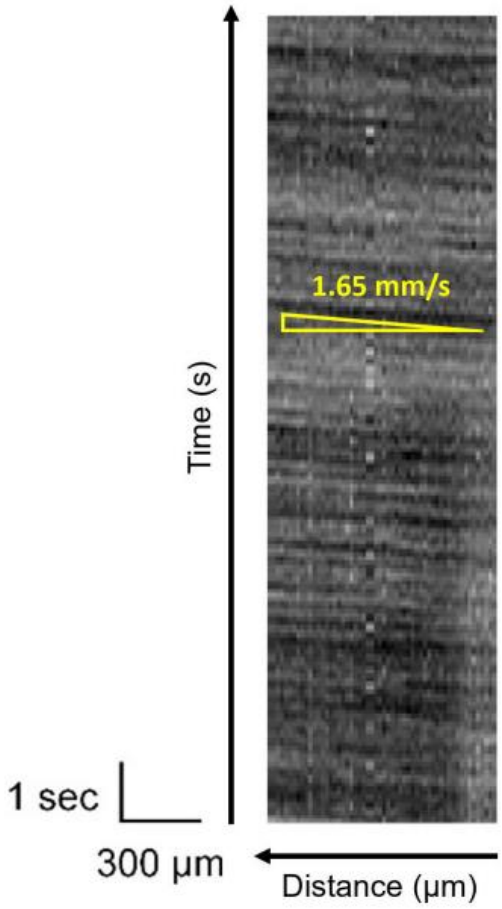

Figure 57 Line scanning image processed from the self-reset image sensor. The dark strip shows high density of the red blood cell moving along the vessel along the time.

4.5 Discussion

According to the design of an image sensor, the pads for connecting the circuit are typically situated in front of the chip on the same side as the pixel array. This can present difficulties in some instances, particularly in in-vivo contact imaging. The pixel array could not be aligned perfectly or attached closely to the imaging target area. In addition, there is a significant possibility that the wire bonding will be physically damaged along the alignment. Consequently, a fiber optic plate (FOP) is used. The FOP is composed of micron-sized optical fibers in the bundle. The incident image from one FOP end face was transferred to the opposing face. The FOP helps to raise the imaging surface above the wire bonding. It shields the wire-bonding point from physical damage and improves the device alignment conditions. However, it was confirmed that there was no significant error or noise due to using FOP throughout the process.

After confirming that the image sensor was properly aligned to the imaging target area using the CISS-NAIST program's live view, the resetting numbers can be counted by increasing the light intensity. However, the reset counting gets harder when the light intensity goes very high. However, when the light intensity goes very high, the reset counting gets harder in case of the exact number the reset counting is required. With this high SNR, it was found that the imaging data suffers from the heartbeats and breathing that cause noise. Thus, an additional technique was required to improve the reconstructed image quality.

Using FOP in this imaging device, almost sufficient spatial resolution was obtained with a pixel size of 15 μm square. In addition, almost no additional noise due to mounting on the living body was observed. For pulsating noise, the frequency component was removed using FFT. Clear improvements were seen in the captured images. The range of brightness is ± 1%, and the result

shows that slight changes in brightness can be observed. However, this technique can only be used in post-processing. In order to observe in real-time during the experiment, it is necessary to introduce a digital filtering technique.

In **Figure 57**, due to the high SNR, the change in brightness due to the concentration of red blood cells in the blood vessels is visible. In this experiment, the frame rate was set to 15 fps. The resolution of the flow velocity can be improved by increasing the brightness of the light source and improving the frame rate. However, it is necessary to consider the effect of heat on the observation target.

4.6 Summary

So far, the blood flow imaging has succeeded using the new self-reset image sensor. The imaging processing was conducted using the subtraction of the reference frame. Thus, the different light intensities between frames were emphasized, and the blood cells moving along the blood vessel were clearly observed. According to the characteristics of the pixel, the lookup table was applied to compensate for the nonlinearity. In addition, the fast Fourier transform method was utilized to bring about a gradual reduction in the pulsating noise. With the use of these imaging results, the velocity of the blood could be measured.

Chapter 5 Conclusion, and Future of this work

5.1 Conclusion

I successfully designed and fabricated a self-resetting image sensor with an SNR of over 70 dB. The pixels with a higher FWC were designed to reduce the self-reset frequency and improve operating stability. Both versions of the pixel have mostly identical performance in terms of SNR. This is due to the photon shot noise limit, as shown in **Figure 58**. However, the result is that enhancing by introducing MOS capacitor provides better linearity, which could benefit imaging and image processing. The new relay boards help get rid of the SNR drop at the first self-resetting as the evaluation result was shown in **Figure 40**. By stabilizing the reset voltage during self-reset, additional noise from self-resetting was decreased by about 4 dB. Thus, the maximum efficiency SNR can be acquired.

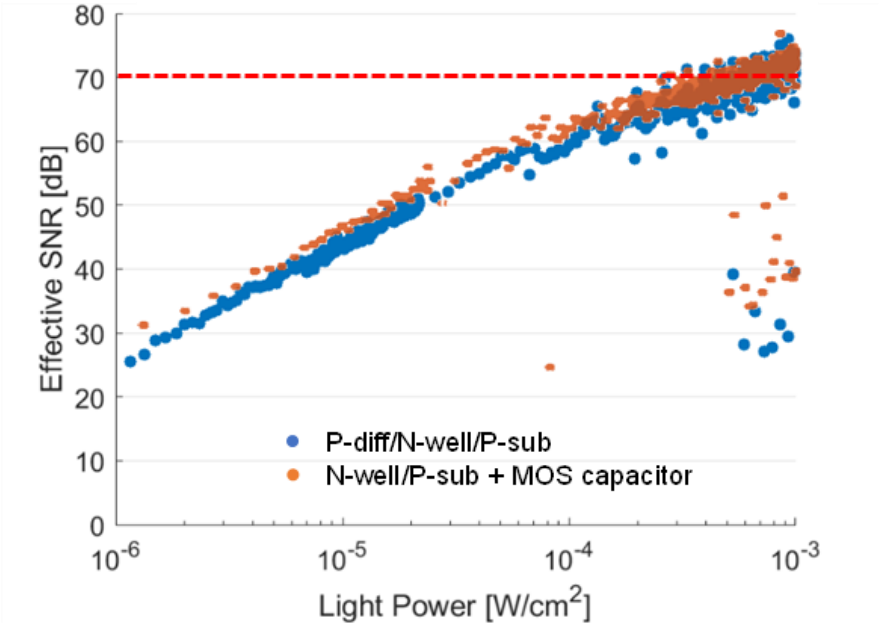

Figure 58 Effective SNR of the fabricated chips. Both versions reach 70 dB.

To summarize the development of this study, the improvements are shown in Table VI. The result shows that the pixel with the MOS capacitor has the most balanced properties improvement since it could achieve such a high SNR of over 70 dB with the moderate stability of the self-resetting system due to the FWC size. However, it offers better linearity compared to the other generations.

Table VI comparison between generations of the self-reset image sensor

	Generation 1 [7]	Generation 2 [50]	Generation 3
Photodiode	N-well/P-sub	P+/N-well + N-well/P-sub	N-well/P-sub + MOS capacitor
FWC	0.19 Me^-	0.72 Me^-	0.3 Me^-
Performance	**Low FWC, Low stability**	**High FWC, Good stability, but poor linearity**	**Moderate FWC, Good stability, and good linearity**

The comparison between this work and the other existing self-reset image sensor is shown in Table VII. Within this study, the image processing script was also developed and be able to extract the intrinsic signal from the data acquired by these self-reset image sensors. This prototype device is tiny enough to be put on the mouse head. It is envisaged that it can be used to observe brain activity linked with diverse behaviors.

Table VII Comparison of the existing self-reset image sensor

	[47]	[48]	[40]	[49]	**This Work**
Technology (μm)	0.25	0.35	0.18	0.50	**0.35**
Tr./pixel	N/A	N/A	43	28	**10**
Pixel size (μm^2)	45 × 45	25 × 25	19 × 19	49 × 49	**15 × 15**
Self-reset type	Comparator	Comparator	Comparator	Schmitt trigger	**Schmitt trigger**
Counter	8-bit	1-bit	6-bit	6-bit	**-**
Fill factor	23%	27%	50%	25%	**30%**
Maximum frame rate	1 kHz	15 kHz	1 kHz	> 1 kHz	**300 Hz**
Peak SNR	N/A	74.5 dB	55.6 dB	65 dB	**> 70 dB**

5.2 Future of this work

As it proved that the self-resetting strategy has the potential to realize such an ideal device for the specific application like an in-vivo imaging. this strategy could be improved by using a finer process, which would result in a higher spatial resolution and larger fill factor. Thus, the device aims to have a larger FWC which means higher stability.

Compared to the pixel applying LOFIC technique [29], [30], which fabricated with 0.18 μm 1-Poly-Si 5-Metal process, the image sensor can achieve 70 dB with 16 μm pixel pitch and 52.8% fill factor. However, 30% of the pixel area was occupied by the capacitor for the LOFIC circuit. With this condition, our self-resetting system design would occupy smaller area, which means the other parameters could be optimized, such as larger fill factor which enlarged FWC, or including the other noise reducing circuit with optimized fill factor.

The successful development of back-illuminated (BI) image sensors was a major turning point for CMOS image sensor technology, enabling the developments of structure for image

sensors. In the first front-illuminated (FI) structures as shown in **Figure 59(a)**, light had to pass through a gap between metal wires to reach a photodiode. With this limitation, it was hard to make the pixel size of the sensor smaller. By the BI structure in **Figure 59(b)**, this allows more light to be collected at the pixel. The resulting images have less digital noise, and the performance can be highly improved.

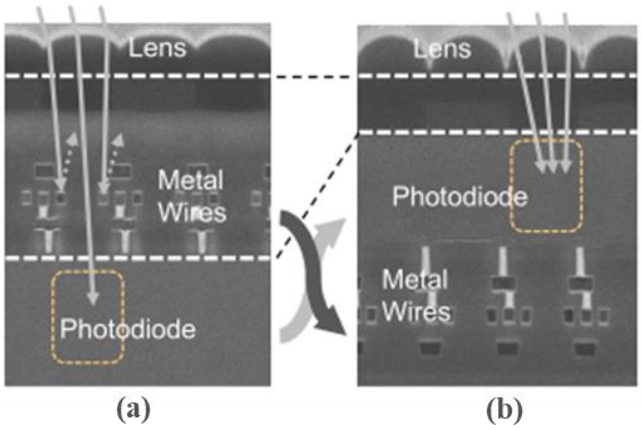

Figure 59 (a) Front illuminated structure, (b) Back illuminated structure [51]**.**

According to this advanced fabrication process, it is able to realize a stacked structure as shown in **Figure 60**. This time the chip is provided as top and bottom part, or even more than two layers [52].

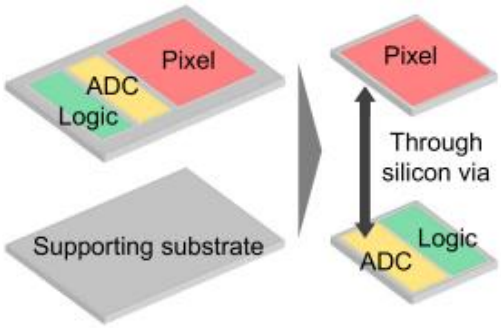

Figure 60 diagram shows the evolution of the image sensor with a stacked structure [51]**.**

Using this technology, the self-reset image sensor could be advantageous from the bottom part as it could include other circuits or techniques to provide more FWC to the pixel. However, this capability is up to the limitations of the process scale. Since the separated part of the chip needs to connect through the via connector. The fine-pitch Cu-Cu connection has been proposed [51]. The present pitch was reduced to 1 μm as shown in **Figure 61**.

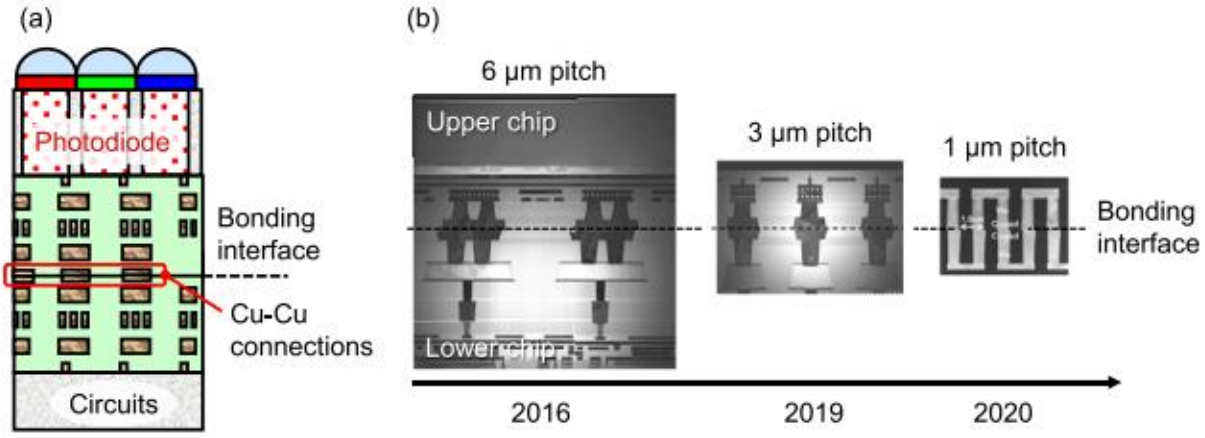

Figure 61 Development of Cu-Cu connection. (a) Diagram shows the bonding interface of the Cu-Cu connection and (b) Trend of the connector pitch [51]**.**

With this cutting-edge technology, the self-resetting pixel technique would be able to implement more complex circuits to enhance its performance. Providing more FWC may be applicable if the pixel size and fabrication process scale are optimally balanced.

References

[1] S. A. Kim and S. B. Jun, “In-vivo Optical Measurement of Neural Activity in the Brain,” *Exp Neurobiol*, vol. 22, no. 3, pp. 158–166, Sep. 2013, doi: 10.5607/en.2013.22.3.158.

[2] M. L. Rynes *et al.*, “Miniaturized head-mounted microscope for whole-cortex mesoscale imaging in freely behaving mice,” *Nat Methods*, vol. 18, no. 4, pp. 417–425, Apr. 2021, doi: 10.1038/s41592-021-01104-8.

[3] T. H. Murphy *et al.*, “High-throughput automated home-cage mesoscopic functional imaging of mouse cortex,” *Nat Commun*, vol. 7, no. 1, p. 11611, Sep. 2016, doi: 10.1038/ncomms11611.

[4] J. Sawinski, D. J. Wallace, D. S. Greenberg, S. Grossmann, W. Denk, and J. N. D. Kerr, “Visually evoked activity in cortical cells imaged in freely moving animals,” *Proceedings of the National Academy of Sciences*, vol. 106, no. 46, pp. 19557–19562, Nov. 2009, doi: 10.1073/pnas.0903680106.

[5] K. K. Ghosh *et al.*, “Miniaturized integration of a fluorescence microscope,” *Nat Methods*, vol. 8, no. 10, pp. 871–878, Oct. 2011, doi: 10.1038/nmeth.1694.

[6] F. Helmchen, M. S. Fee, D. W. Tank, and W. Denk, “A Miniature Head-Mounted Two-Photon Microscope,” *Neuron*, vol. 31, no. 6, pp. 903–912, Sep. 2001, doi: 10.1016/S0896-6273(01)00421-4.

[7] T. Yamaguchi *et al.*, “Implantable self-reset CMOS image sensor and its application to hemodynamic response detection in living mouse brain,” *Jpn J Appl Phys*, vol. 55, no. 4S, p. 04EM02, Apr. 2016, doi: 10.7567/JJAP.55.04EM02.

[8] T.-W. Chen *et al.*, “Ultrasensitive fluorescent proteins for imaging neuronal activity,” *Nature*, vol. 499, no. 7458, pp. 295–300, Jul. 2013, doi: 10.1038/nature12354.

[9] C. Grienberger and A. Konnerth, “Imaging Calcium in Neurons,” *Neuron*, vol. 73, no. 5, pp. 862–885, Mar. 2012, doi: 10.1016/j.neuron.2012.02.011.

[10] M. J. Berridge, P. Lipp, and M. D. Bootman, “The versatility and universality of calcium signalling,” *Nat Rev Mol Cell Biol*, vol. 1, no. 1, pp. 11–21, Oct. 2000, doi: 10.1038/35036035.

[11] O. Skocek *et al.*, “High-speed volumetric imaging of neuronal activity in freely moving rodents,” *Nat Methods*, vol. 15, no. 6, pp. 429–432, Jun. 2018, doi: 10.1038/s41592-018-0008-0.

[12] W. Zong *et al.*, “Fast high-resolution miniature two-photon microscopy for brain imaging in freely behaving mice,” *Nat Methods*, vol. 14, no. 7, pp. 713–719, Jul. 2017, doi: 10.1038/nmeth.4305.

[13] I. Ferezou, S. Bolea, and C. C. H. Petersen, “Visualizing the Cortical Representation of Whisker Touch: Voltage-Sensitive Dye Imaging in Freely Moving Mice,” *Neuron*, vol. 50, no. 4, pp. 617–629, May 2006, doi: 10.1016/j.neuron.2006.03.043.

[14] C. Martin, J. Martindale, J. Berwick, and J. Mayhew, “Investigating neural–hemodynamic coupling and the hemodynamic response function in the awake rat,” *Neuroimage*, vol. 32, no. 1, pp. 33–48, Aug. 2006, doi: 10.1016/j.neuroimage.2006.02.021.

[15] T. Matsuura, H. Fujita, K. Kashikura, and I. Kanno, “Evoked local cerebral blood flow induced by somatosensory stimulation is proportional to the baseline flow,” *Neurosci Res*, vol. 38, no. 4, pp. 341–348, Dec. 2000, doi: 10.1016/S0168-0102(00)00175-9.

[16] M. Takahashi *et al.*, “Imaging of Neuronal Activity in Awake Mice by Measurements of Flavoprotein Autofluorescence Corrected for Cerebral Blood Flow,” *Front Neurosci*, vol. 11, no. JAN, pp. 1–8, Jan. 2018, doi: 10.3389/fnins.2017.00723.

[17] J. Nakai, M. Ohkura, and K. Imoto, “A high signal-to-noise Ca2+ probe composed of a single green fluorescent protein,” *Nat Biotechnol*, vol. 19, no. 2, pp. 137–141, Feb. 2001, doi: 10.1038/84397.

[18] K. Shibuki *et al.*, “Dynamic Imaging of Somatosensory Cortical activity in the Rat Visualized by Flavoprotein Autofluorescence,” *J Physiol*, vol. 549, no. 3, pp. 919–927, Jun. 2003, doi: 10.1113/jphysiol.2003.040709.

[19] D. C. Ng *et al.*, “A Complementary Metal–Oxide–Semiconductor Image Sensor for On-Chip *in Vitro* and *in Vivo* Imaging of the Mouse Hippocampus,” *Jpn J Appl Phys*, vol. 45, no. 4B, pp. 3799–3806, Apr. 2006, doi: 10.1143/JJAP.45.3799.

[20] A. Tagawa *et al.*, “Development of Complementary Metal Oxide Semiconductor Imaging Devices for Detecting Green Fluorescent Protein in the Deep Brain of a Freely Moving Mouse,” *Jpn J Appl Phys*, vol. 48, no. 4, p. 04C195, Apr. 2009, doi: 10.1143/JJAP.48.04C195.

[21] T. Kobayashi *et al.*, “Potentiometric Dye Imaging for Pheochromocytoma and Cortical Neurons with a Novel Measurement System Using an Integrated Complementary Metal–

Oxide–Semiconductor Imaging Device," *Jpn J Appl Phys*, vol. 49, no. 11, p. 117001, Nov. 2010, doi: 10.1143/JJAP.49.117001.

[22] T. Kobayashi *et al.*, "Novel implantable imaging system for enabling simultaneous multiplanar and multipoint analysis for fluorescence potentiometry in the visual cortex," *Biosens Bioelectron*, vol. 38, no. 1, pp. 321–330, Oct. 2012, doi: 10.1016/j.bios.2012.06.035.

[23] J. Ohta, T. Tokuda, K. Sasagawa, and T. Noda, "Implantable CMOS Biomedical Devices," *Sensors*, vol. 9, no. 11, pp. 9073–9093, Nov. 2009, doi: 10.3390/s91109073.

[24] M. Haruta *et al.*, "An implantable CMOS device for blood-flow imaging during experiments on freely moving rats," *Jpn J Appl Phys*, vol. 53, no. 4S, p. 04EL05, Jan. 2014, doi: 10.7567/JJAP.53.04EL05.

[25] M. Haruta *et al.*, "Chronic brain blood-flow imaging device for a behavioral experiment using mice," *Biomed Opt Express*, vol. 10, no. 4, p. 1557, Apr. 2019, doi: 10.1364/BOE.10.001557.

[26] M. Haruta *et al.*, "Intrinsic signal imaging of brain function using a small implantable CMOS imaging device," *Jpn J Appl Phys*, vol. 54, no. 4S, p. 04DL10, Apr. 2015, doi: 10.7567/JJAP.54.04DL10.

[27] J. Nakamura, *Image sensors and signal processing for digital still cameras*. 2017. doi: 10.1201/9781420026856.

[28] G. Meynants *et al.*, “700 frames/s 2 MPixel global shutter image sensor with 2 Me- full well charge and 12 μm pixel pitch,” *proc. International Image Sensor workshop*, pp. 409–413, 2015.

[29] N. Akahane, S. Sugawa, S. Adachi, K. Mori, T. Ishiuchi, and K. Mizobuchi, “A sensitivity and linearity improvement of a 100-dB dynamic range CMOS image sensor using a lateral overflow integration capacitor,” in *IEEE Journal of Solid-State Circuits*, 2006, vol. 41, no. 4. doi: 10.1109/JSSC.2006.870753.

[30] Y. Fujihara, M. Murata, S. Nakayama, R. Kuroda, and S. Sugawa, “An Over 120 dB Single Exposure Wide Dynamic Range CMOS Image Sensor With Two-Stage Lateral Overflow Integration Capacitor,” *IEEE Trans Electron Devices*, vol. 68, no. 1, pp. 152–157, Jan. 2021, doi: 10.1109/TED.2020.3038621.

[31] M. Loose, K. Meier, and J. Schemmel, “A Self-Calibrating Single-Chip CMOS Camera with Logarithmic Response,” vol. 36, no. 4, pp. 586–596, 2001.

[32] C. C. A. D. Converters, M. Mase, S. Kawahito, S. Member, M. Sasaki, and Y. Wakamori, “A Wide Dynamic Range CMOS Image Sensor With Multiple Exposure-Time Signal Outputs and,” vol. 40, no. 12, pp. 2787–2795, 2005.

[33] O. Yadid-pecht, E. R. Fossum, and S. Member, “Wide Intrascene Dynamic Range CMOS APS Using Dual Sampling,” vol. 44, no. 10, pp. 1721–1723, 1997.

[34] J. G. Harris, “A TIME-BASED CMOS IMAGE SENSOR”.

[35] A. Kitchen, A. Bermak, and A. Bouzerdoum, “PWM digital pixel sensor based on asynchronous self-resetting scheme,” *IEEE Electron Device Letters*, vol. 25, no. 7, pp. 471–473, 2004, doi: 10.1109/LED.2004.831222.

[36] D. Park, J. Rhee, and Y. Joo, “A wide dynamic-range CMOS image sensor using self-reset technique,” *IEEE Electron Device Letters*, vol. 28, no. 10, pp. 890–892, 2007, doi: 10.1109/LED.2007.905396.

[37] A. Bermak, A. Bouzerdoum, and K. Eshraghian, “A vision sensor with on-pixel ADC and in-built light adaptation mechanism,” *Microelectronics J*, vol. 33, no. 12, pp. 1091–1096, 2002, doi: 10.1016/S0026-2692(02)00114-3.

[38] J. Yuan, H. Y. Chan, S. W. Fung, and B. Liu, “An activity-triggered 95.3 dB DR - 75.6 dB THD CMOS imaging sensor with digital calibration,” *IEEE J Solid-State Circuits*, vol. 44, no. 10, pp. 2834–2843, 2009, doi: 10.1109/JSSC.2009.2027929.

[39] S. Koppa, D. Park, Y. Joo, and S. Jung, “A 105.6dB DR and 65dB peak SNR self-reset CMOS image sensor using a Schmitt trigger circuit,” *Midwest Symposium on Circuits and Systems*, 2011, doi: 10.1109/MWSCAS.2011.6026323.

[40] D. Park, J. Rhee, and Y. Joo, “A Wide Dynamic-Range CMOS Image Sensor Using Self-Reset Technique,” *IEEE Electron Device Letters*, vol. 28, no. 10, pp. 890–892, Oct. 2007, doi: 10.1109/LED.2007.905396.

[41] A. Kitchen, A. Bermak, and A. Bouzerdoum, “PWM Digital Pixel Sensor Based on Asynchronous Self-Resetting Scheme,” *IEEE Electron Device Letters*, vol. 25, no. 7, pp. 471–473, Jul. 2004, doi: 10.1109/LED.2004.831222.

[42] K. Sasagawa *et al.*, “An implantable image sensor with self-reset function for brain imaging,” *IEEE 2014 Biomedical Circuits and Systems Conference, BioCAS 2014 - Proceedings*, pp. 252–255, 2014, doi: 10.1109/BioCAS.2014.6981710.

[43] K. Sasagawa *et al.*, “An implantable CMOS image sensor with self-reset pixels for functional brain imaging,” *IEEE Trans Electron Devices*, vol. 63, no. 1, pp. 215–222, 2016, doi: 10.1109/TED.2015.2454435.

[44] T. Yamaguchi *et al.*, “Implantable self-reset CMOS image sensor and its application to hemodynamic response detection in living mouse brain,” *Jpn J Appl Phys*, vol. 55, no. 4, 2016, doi: 10.7567/JJAP.55.04EM02.

[45] K. Sasagawa *et al.*, “Hemodynamic imaging using an implantable self-reset image sensor,” *Proceedings - 2016 IEEE Biomedical Circuits and Systems Conference, BioCAS 2016*, no. 26249051, pp. 452–455, 2016, doi: 10.1109/BioCAS.2016.7833829.

[46] K. Sasagawa *et al.*, “Hemodynamic imaging using an implantable self-reset image sensor,” in *2016 IEEE Biomedical Circuits and Systems Conference (BioCAS)*, Oct. 2016, no. 26249051, pp. 452–455. doi: 10.1109/BioCAS.2016.7833829.

[47] A. Bermak, A. Bouzerdoum, and K. Eshraghian, “A vision sensor with on-pixel ADC and in-built light adaptation mechanism,” *Microelectronics J*, vol. 33, no. 12, pp. 1091–1096, Dec. 2002, doi: 10.1016/S0026-2692(02)00114-3.

[48] J. Yuan, H. Y. Chan, S. W. Fung, and B. Liu, “An Activity-Triggered 95.3 dB DR $-$75.6 dB THD CMOS Imaging Sensor With Digital Calibration,” *IEEE J Solid-State Circuits*, vol. 44, no. 10, pp. 2834–2843, Oct. 2009, doi: 10.1109/JSSC.2009.2027929.

[49] S. Koppa, D. Park, Y. Joo, and S. Jung, “A 105.6dB DR and 65dB peak SNR self-reset CMOS image sensor using a Schmitt trigger circuit,” in *2011 IEEE 54th International Midwest Symposium on Circuits and Systems (MWSCAS)*, Aug. 2011, pp. 1–4. doi: 10.1109/MWSCAS.2011.6026323.

[50] T. Pakpuwadon *et al.*, “Self-Reset Image Sensor With a Signal-to-Noise Ratio Over 70 dB and Its Application to Brain Surface Imaging,” *Front Neurosci*, vol. 15, no. June, pp. 1–11, Jun. 2021, doi: 10.3389/fnins.2021.667932.

[51] Y. Oike, “Evolution of Image Sensor Architectures With Stacked Device Technologies,” *IEEE Trans Electron Devices*, vol. 69, no. 6, 2022, doi: 10.1109/TED.2021.3097983.

[52] T. Haruta *et al.*, “A 1/2.3inch 20Mpixel 3-layer stacked CMOS Image Sensor with DRAM,” in *Digest of Technical Papers - IEEE International Solid-State Circuits Conference*, 2017, vol. 60. doi: 10.1109/ISSCC.2017.7870268.

List of Publications

Journal :

- Pakpuwadon, T., Sasagawa, K., Guinto, M. C., Ohta, Y., Haruta, M., Takehara, H., Tashiro, H., & Ohta, J. (2021). Self-Reset Image Sensor With a Signal-to-Noise Ratio Over 70 dB and Its Application to Brain Surface Imaging. Frontiers in neuroscience, 15, 667932.

Conference :

- Pakpuwadon Thanet, Mark Christian Guinto, Makito Haruta, Hironari Takehara, Hiroyuki Tashiro, Kiyotaka Sasagawa, Jun Ohta, "Linearity improvement of self-reset CMOS image sensor with high signal-to-noise ratio" Annual Conference of the Institute of Electrical Engineers of Japan, March 22, 2022.
- Pakpuwadon Thanet, Kiyotaka Sasagawa, Mark Christian Guinto, Makito Haruta, Hironari Takehara, Hiroyuki Tashiro, Jun Ohta, "A self-reset CMOS imaging device with high capacitance photodiode" The Japan Society of Applied Physics, March 18, 2021.
- Pakpuwadon Thanet, Kiyotaka Sasagawa, Mark Christian Guinto, Makito Haruta, Hironari Takehara, Hiroyuki Tashiro, Jun Ohta, "A self-reset CMOS image sensor for high signal-to-noise in-vivo imaging" International Conference on Solid State Devices and Materials (SSDM2020), September 30, 2020.
- Pakpuwadon Thanet, Kiyotaka Sasagawa, Mark Christian Guinto, Makito Haruta, Hironari Takehara, Hiroyuki Tashiro, Jun Ohta, "A self-reset image sensor with a high

signal-to-noise ratio for in vivo-experiment" , d.lab-VDEC デザイナーズフォーラム, September 25, 2020.